A MODEL FOR THE SATELLITE AERONAUTICAL TAXIING CHANNEL

F.P.Fontan, B.Sanmartin, A.Steingass, A.Lehner and J.J.Navarro

[(1)]*Universidad de Vigo, ETSE Telecomunicación, Campus Universitario. 36200, Vigo, Spain, fpfontan@tsc.uvigo.es, bsanper@tsc.uvigo.es*

[(2)]*German Aerospace Center (DLR), Institute for Communications and Navigation, D-82230 Wessling, Germany, alexander.steingass@dlr.de, andreas.lehner@dlr.de*

[(3)]*AENA (Aeropuertos Españoles y Navegación Aérea). Division de Navegación y Vigilancia Josefa Varcarcel 30. 280027 Madrid. Spain. jjnavarro@aena.es*

1 INTRODUCTION

In this paper a channel model for the satellite to aircraft channel during the taxiing phase is presented. Great importance is being given to airport surface operations during low visibility conditions. Airport capacity might be limited during low visibility conditions as the ease of aircraft to move from/to the runway to/from the apron can be greatly reduced. New systems are being developed to improve airport capacity under the concept of Advanced Surface Movement Guidance and Control Systems (A-SMGCS) [1]. The control and monitoring of taxiway traffic requires determining the position of all aircraft during the taxiing phase. Satellite navigation signals are a fundamental source of position information which might be impaired by the existing multipath in the taxiing area.

This paper presents a hybrid physical-statistical model that attempts to accurately reproduce propagation conditions during this phase. First, aircraft originated multipath is modeled using physical optics, PO, techniques. Radar cross section results for various aircraft are evaluated for all possible incidence angles and stored for later use. Furthermore, the assumption is made that the scattering angle, θ_s, for any given aircraft to the interfered one is constant and equal to 90º. This greatly facilitates the study: incidence angles, θ_i and ϕ_i, can be discretized with a step of 10º and bi-static RCS values computed for such discrete values of ϕ_i assuming, θ_s, = 90º.

In a second step, a statistical model is developed assuming that the various aircraft are point scatterers (sources of multipath) and using the RCS values already calculated and stored. Several operational scenarios can be developed by deploying point scatterers on the simulation scenario and assuming given mobility patterns.

The model presented is wide-band thus providing information on the time-spreading characteristics of the channel. Tapped delay-lines can also be produced consisting of a number of time-delayed complex time-series conveying the signal fading and Doppler introduced by the elements present in the assumed generic taxiing scenario.

2 MODEL ELEMENTS. DETERMINISTIC MODELING

The main model elements involved in the satellite aeronautical propagation channel when the aircraft is in the taxiing phase are the aircraft itself, other aircraft queuing up (in-sequence) on their way to/from the runway, and the ground. As a first approximation, it can be assumed that the victim

aircraft is not near large structures such as the terminal building. Right hand circular polarization, RHCP, is assumed in this study.

During taxiing, the direct signal will most probably be unblocked and its level will depend on the receive antenna pattern, and the radio path elevation and azimuth. If antenna gain masks are used, an omni-azimuth pattern can be supposed. In this study a low gain antenna of about 3 dBi is assumed. This pattern is plotted in Figure 1 and the general formula for the gain

$$G(\theta) = -4 \times 10^{-4} \left(10^{G_{Max}/10} - 1\right)\theta^2 \quad \text{dB}$$

where θ is in degrees, has been used to describe the antenna pattern [2].

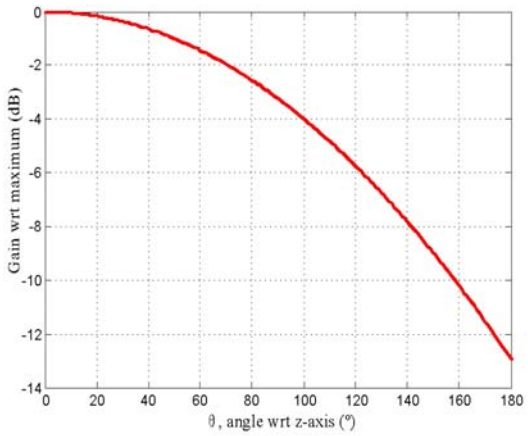

Figure 1. Antenna pattern mask assumed in the model. Maximum gain 3 dBi.

Given that no blockage effects are present, the channel is impaired by multipath. Three main sources have been identified when the victim aircraft is on its way to/from the runway, namely, (1) the multipath originating on the victim aircraft itself: body, wings, etc., (2) the multipath originating on other aircraft nearby, and (3) multipath from the ground.

A study has been carried out to evaluate the receive level of multipath originated multipath. This study has been performed using PO techniques as described in the Annex [3].

At the victim aircraft antenna, the unblocked direct ray is accompanied by reflections originating on parts of aircraft itself. Such reflections and the slow movement of the aircraft during taxiing lead to moderate to very slow-varying fading of the direct signal. A Rice model including a narrow second order Butterworth Doppler spectrum is appropriate for this purpose. A cutoff frequency for the Doppler frequency on the order of 1 Hz is assumed to be a reasonable approximation [3].

Given that the reflections on the cabin, engines, wings, etc. of the aircraft correspond to small sections of curved surfaces, a geometrical optics (GO) approach is not completely valid, i.e., it is not possible to apply directly the Fresnel reflection coefficients.

To overcome the above mentioned limitations, a Physical Optics (PO) [4][5] approach was followed. Thus, the aircraft's external surface was meshed in small triangles whose individual contributions make up the part of the overall channel impulse response due to the aircraft-originated multipath.

The meshing of the aircraft surface (Figure 2) has to fulfill a number of conditions to allow the application of PO techniques. From the system simulation point of view, the mesh grid should be sufficiently small giving rise to delay increments much smaller than the inverse of the system's bandwidth.

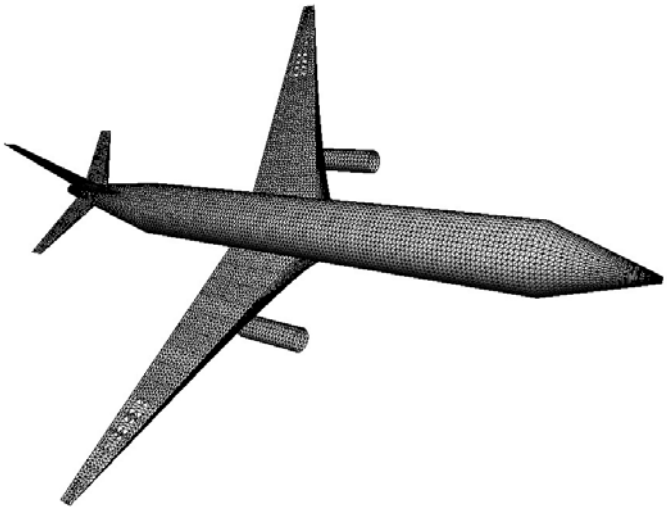

Figure 2. Meshed aircraft.

The PO contributions are complex-valued and their phases change as parts of the aircraft slightly change with respect to each other during taxiing. If these contributions are added coherently to the direct signal, a fading process results.

An electromagnetic study has been carried out for a large aircraft of about 60 m in length and 60 m from wing tip to wing tip [3]. Examples of obtained results are illustrated in Figures 3-9 for different illumination angles. In these figures the magnitude of the ideal (ensemble of deltas) channel impulse response are illustrated.

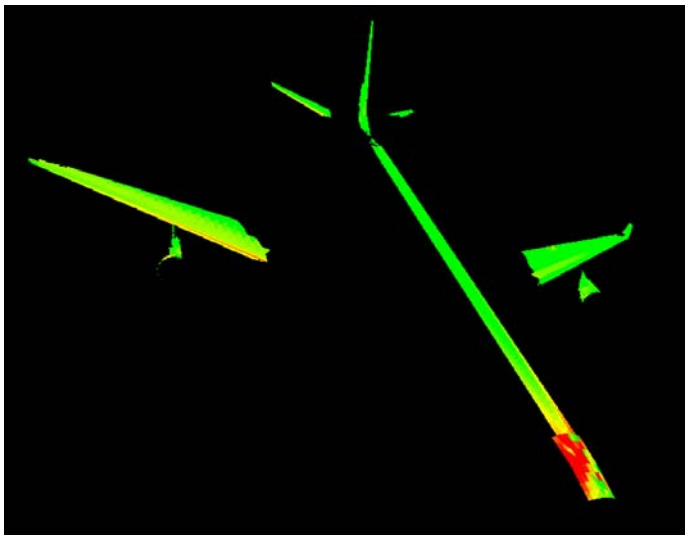

Figure 3. Color coded areas on the simulated aircraft surface contributing to the aircraft originated multipath.

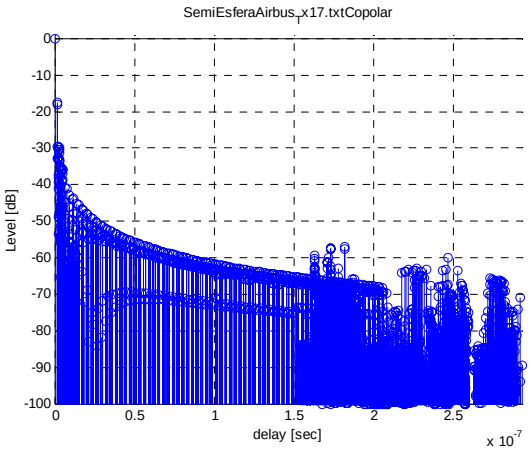

Figure 4. Calculated impulse response for incidence angle: azimuth=-8º, elevation=54º.

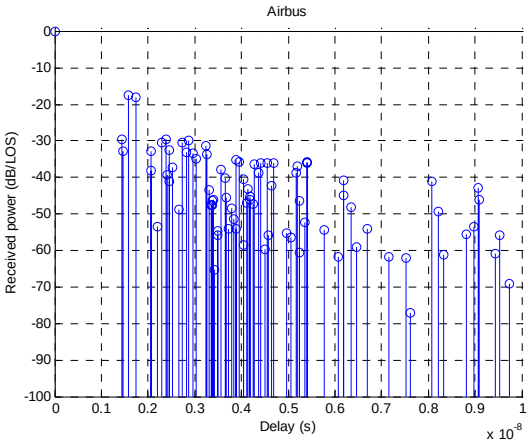

Figure 5. Calculated impulse response for incidence angle: azimuth=-8º, elevation=54º. (Zoomed in)

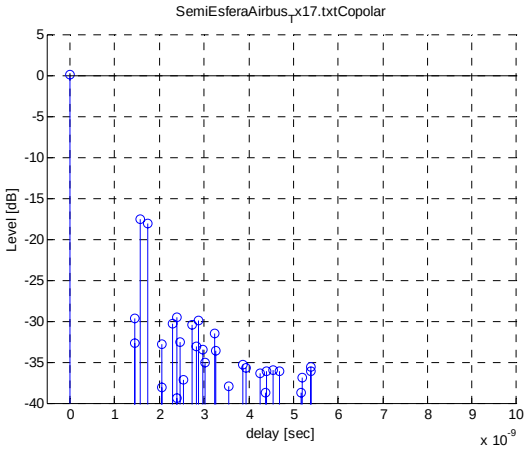

Figure 6. Calculated impulse response for incidence angle: azimuth=-8º, elevation=54º. (Zoomed in)

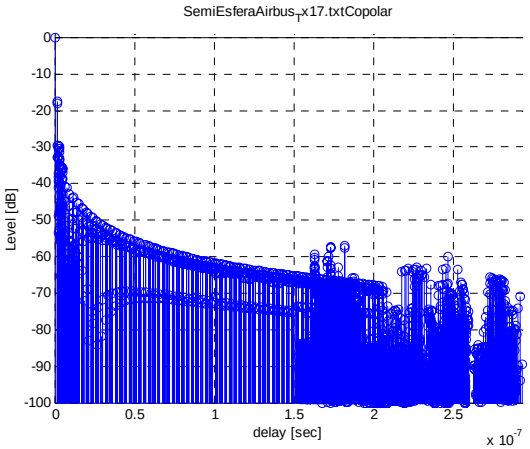

Figure 7. Calculated impulse response for incidence: azimuth=-32º, elevation=9º.

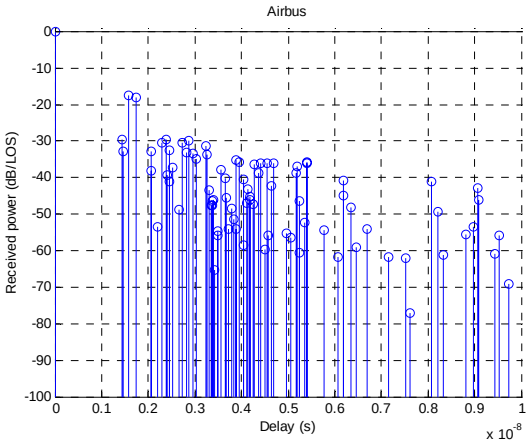

Figure 8. Calculated impulse response for incidence: azimuth=-32º, elevation=9º. (Zoomed in)

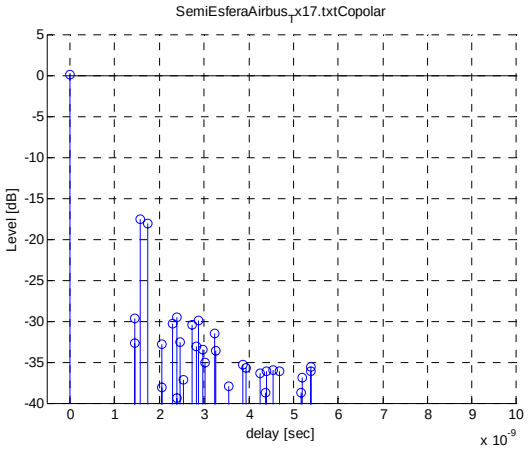

Figure 9. Calculated impulse response for incidence: azimuth=-32º, elevation=9º. (Zoomed in)

Figure 10 illustrates how the incidence angles were sampled and Figure 11 shows the overall power of the various multipath components originating from the body and wings of the aircraft is summarized for all possible incidence angles. This plot gives an indication of the multipath power to be expected to interfere with the direct signal. It can be observed how multipath is stronger for some incidence angles than others. More specifically, for the lower elevation angles, multipath tends to be stronger. If a **worst-case scenario** is to be considered, aircraft multipath powers on the order of -13 dB relative to the direct signal at low elevations should be considered. This means that the first tap (Tap-0) of the TDL model to be produced later on will show a Rice behavior with a carrier-to-multipath parameter, K=13 dB. These assumptions are valid provided that the receive antenna presents isotropic conditions.

The above study was carried out a constant-gain antenna down to 25º below the horizon. For slightly more realistic antennas, the spatial filtering effects introduced by the antenna pattern (Figure 1) will modify this value yielding a more moderate value of -17 dB (K=17 dB) relative power with respect to the direct signal at low elevation angles.

In Figures 4-9 the aircraft originated multipath power corresponds to excess delays up to 300 ns, although significant contributions are only produced for the first few ns. This leads to the conclusion that all aircraft-originated multipath must be included on the first tap (Tap-0) in a Tapped Delay-Line, TDL) model for most envisaged system bandwidths.

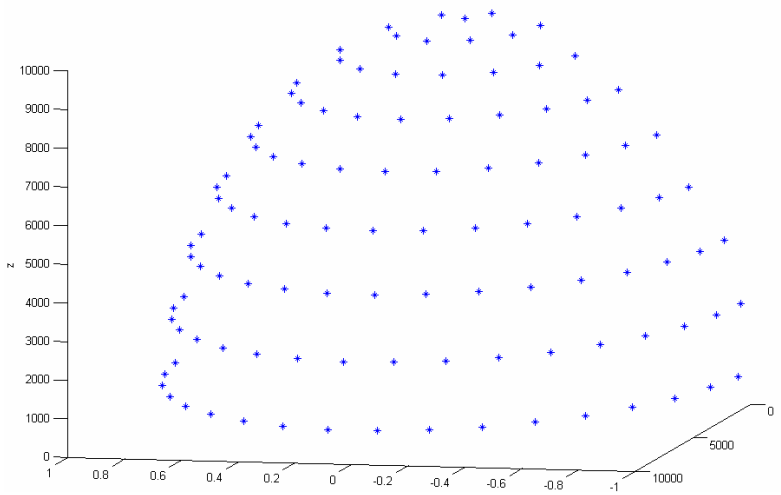

Figure 10. Direction of arrival sampling for calculating the aircraft originated multipath contribution.

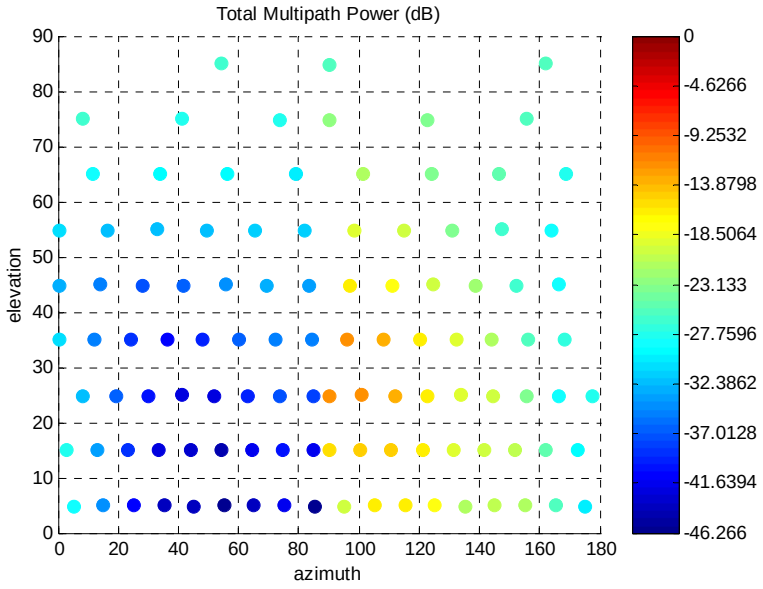

Figure 11. Inverse carrier-to-multipath power ratio, -*K* (dB), for all possible incidence angles. Isotropic antenna down to 25º below the horizontal plane.

Similarly, multipath levels have been calculated for contributions arriving from other aircraft nearby. In this case, given that authorized distances for queuing aircraft during taxiing are on the order of 90 m, it is possible to use the concept of bi-static radar cross section which is defined as

$$\sigma\,(\mathrm{m}^2) = \lim_{R\to\infty} 4\pi R^2 \frac{|E_\mathrm{s}|^2}{|E_\mathrm{i}|^2}$$

where E_i is the incident electric field and E_s is the scattered electrical field and R is the distance to the receiver.

Contrary to the previous case, multiple incidence and scattering angle combinations are possible. This would lead to enormous computation loads and storage. The following simplification has been made: the scattering angle, θ_s, was assumed to be 90º, i.e., 90º from the vertical axis or equivalently, it is assumed that the scattering direction from a neighboring aircraft to the victim aircraft is parallel to the horizontal plane. This reduces drastically the number of calculations and storage space needed.

Figure 12 illustrates the assumed interference configuration where both the victim and an aircraft nearby are shown.

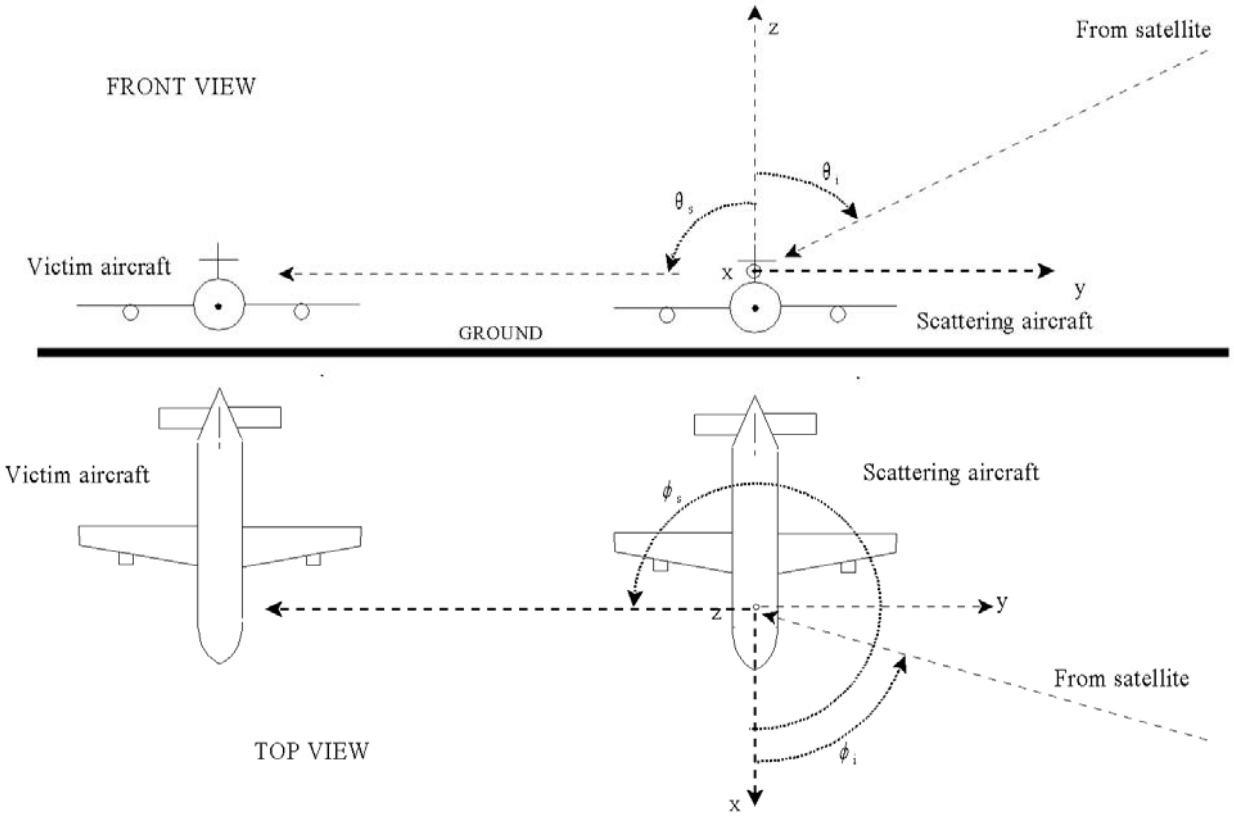

Figure 12. Aircraft to aircraft scattering geometry.

Next an example of the usage of the RCS figures provided below is presented. Assume the situation indicated in Figure 12, where the incidence angles are ϕ_i = 70 degree and θ_i = 60 degree and the scattering angles are ϕ_s = 210 degree and θ_s = 90 degree. Given the symmetry in the aircraft, it is best to choose ϕ_s = 90 (since no plot is provided for ϕ_s = 270) and move the incidence angles to the opposite quadrant, thus, ϕ_i = 360-70 = 290 degree and θ_i = 60 degree. Reading the corresponding RCS value on the corresponding figure for ϕ_s = 90 as illustrated in Figure 13, gives an RCS value of approximately 12 dBm^2.

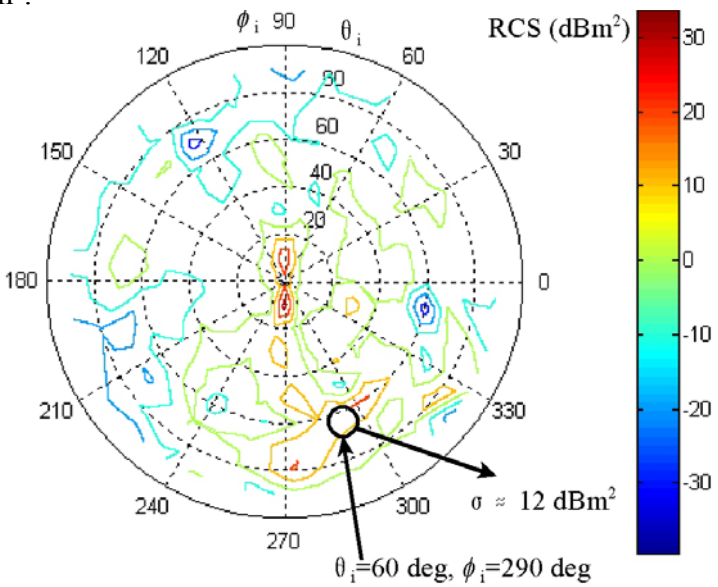

Figure 13. Illustration of use for RCS plots below as a function of the geometry in Figure 12.

Simulated bi-static radar cross-sections for different incidence angles are shown in Figures 14-32. In Figure 33 the maxima for each of the previous plots are shown. Similarly, the average RCSs for each azimuth cut are shown in Figure 34. From these figures, a **worst case scenario** can be defined by considering a constant RCS value of 30 dBm^2 for all possible incidence angles. Other cases (better or worse) can be defined by decreasing or increasing the selected constant RCS value.

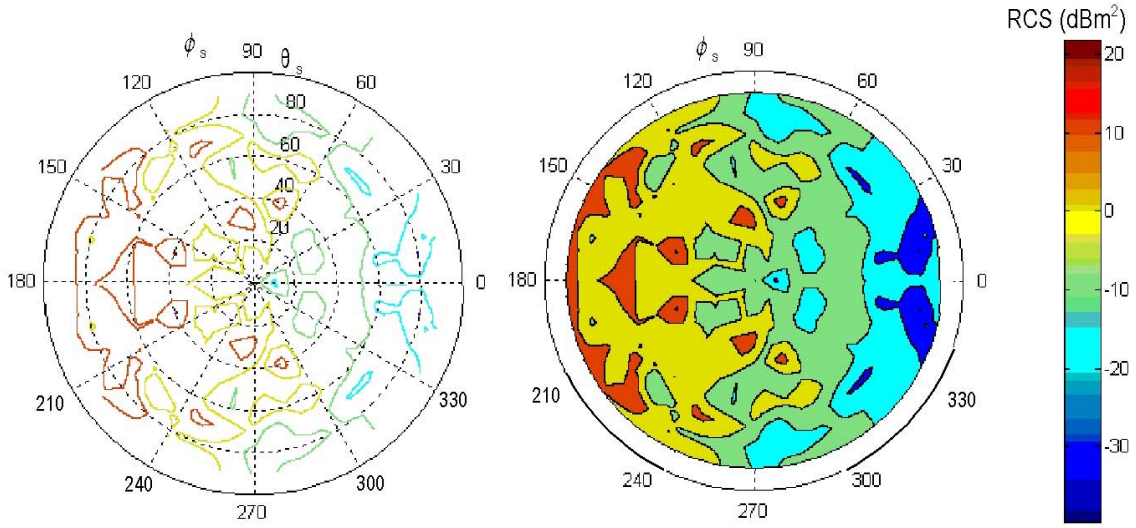

Figure 14. Scattering azimuth $\phi_s = 0^o$

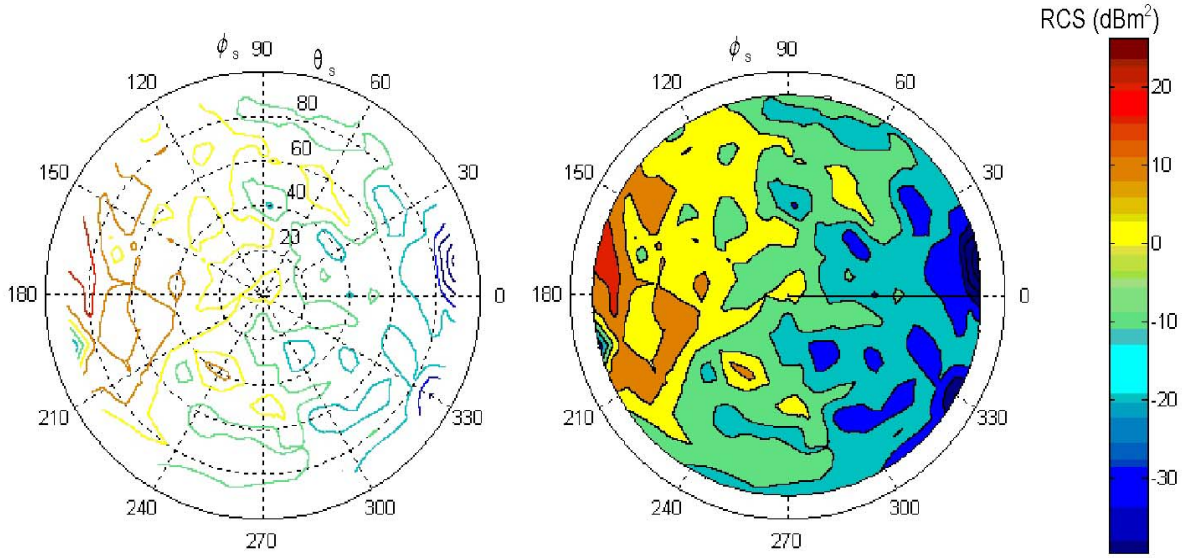

Figure 15. Scattering azimuth $\phi_s = 10^o$

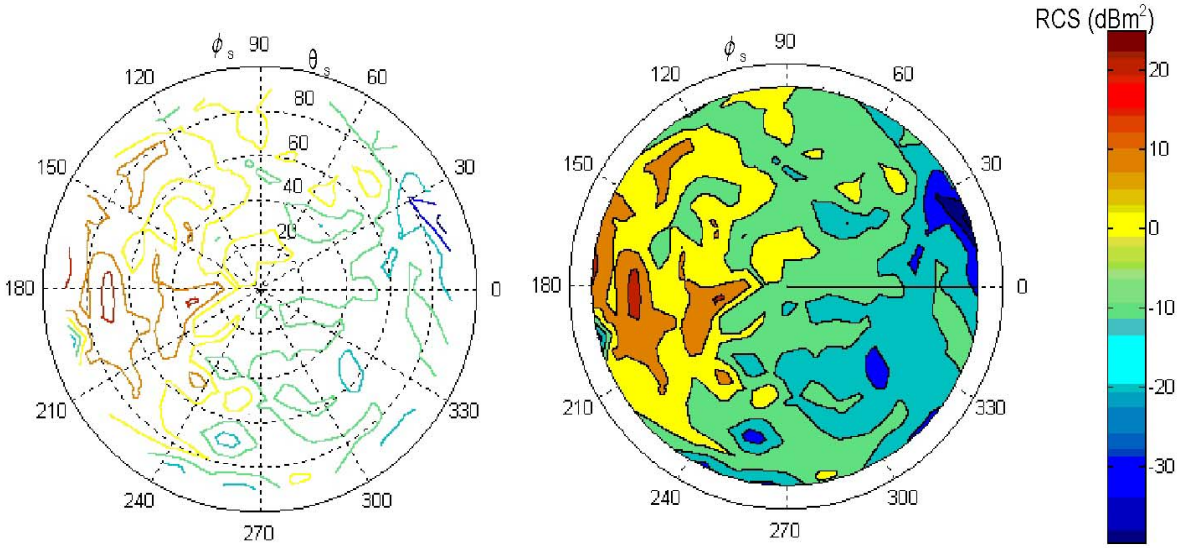

Figure 16. Scattering azimuth $\phi_s = 20^o$

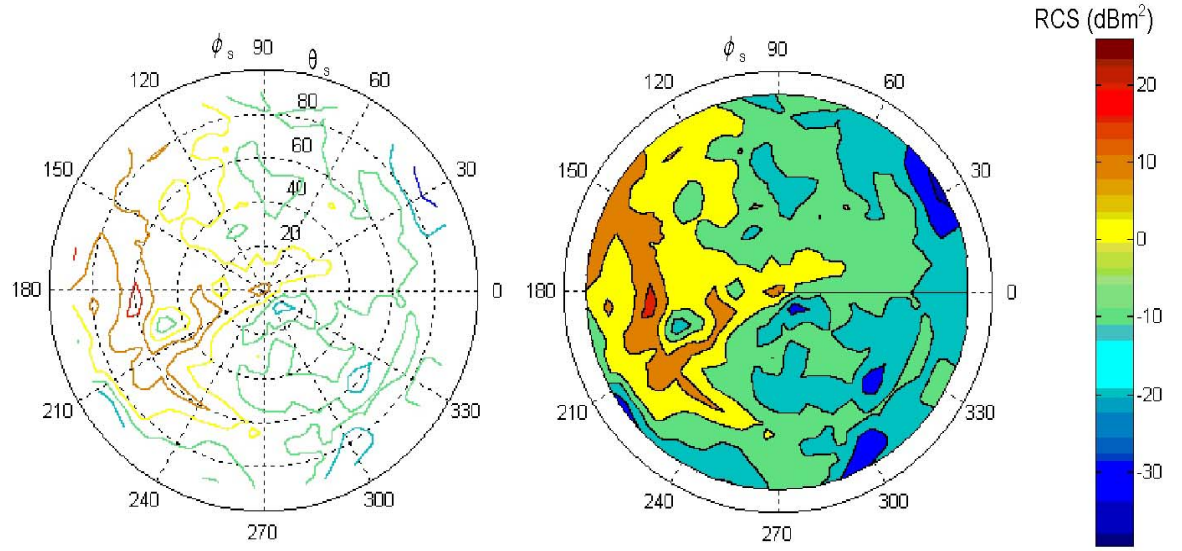

Figure 17. Scattering azimuth $\phi_s = 30^o$

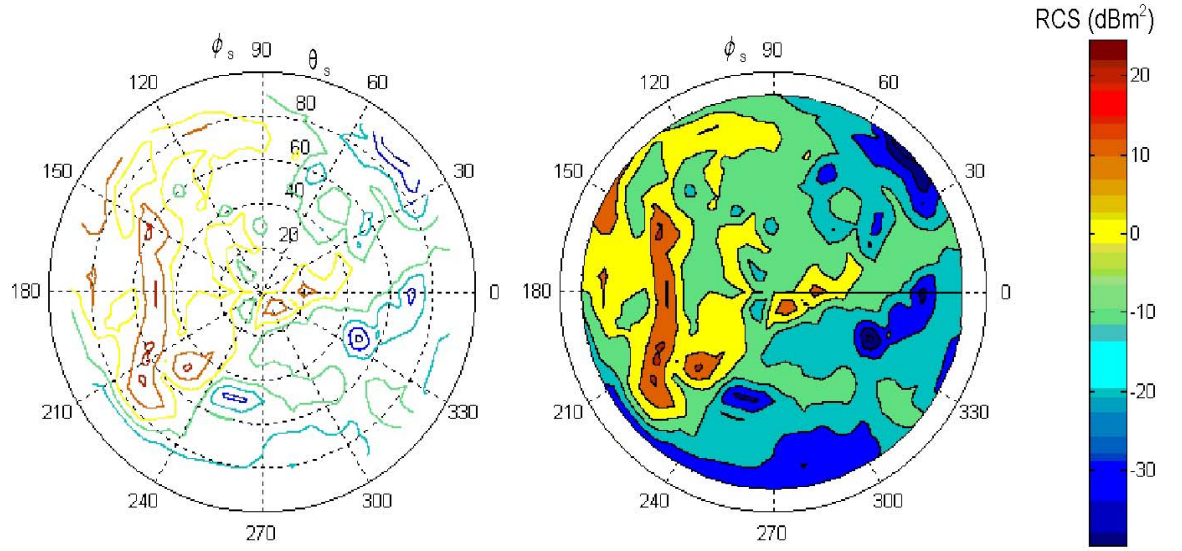

Figure 18. Scattering azimuth $\phi_s = 40^o$

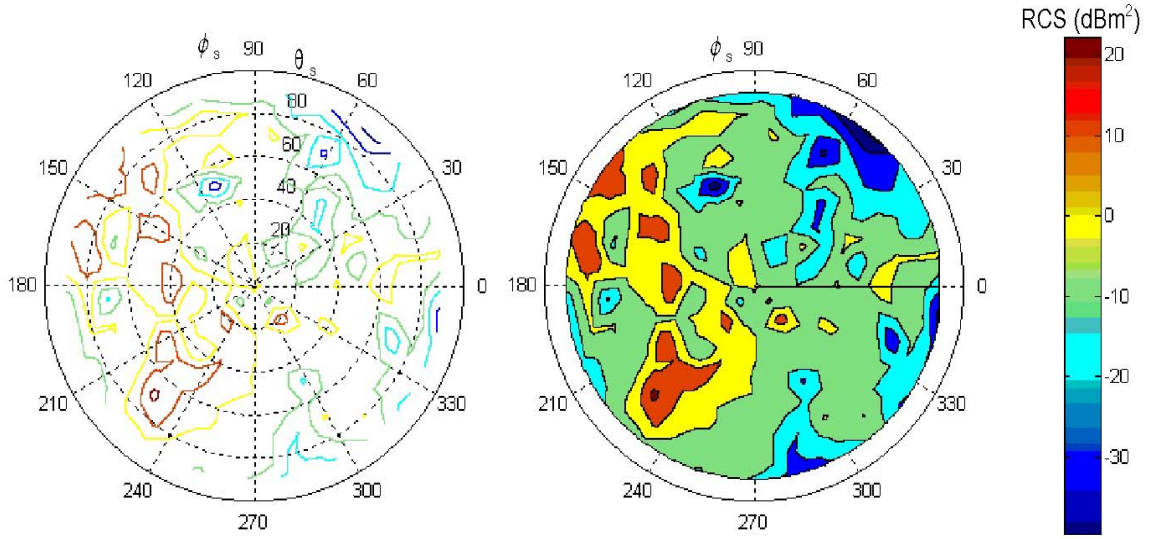

Figure 19. Scattering azimuth $\phi_s = 50°$

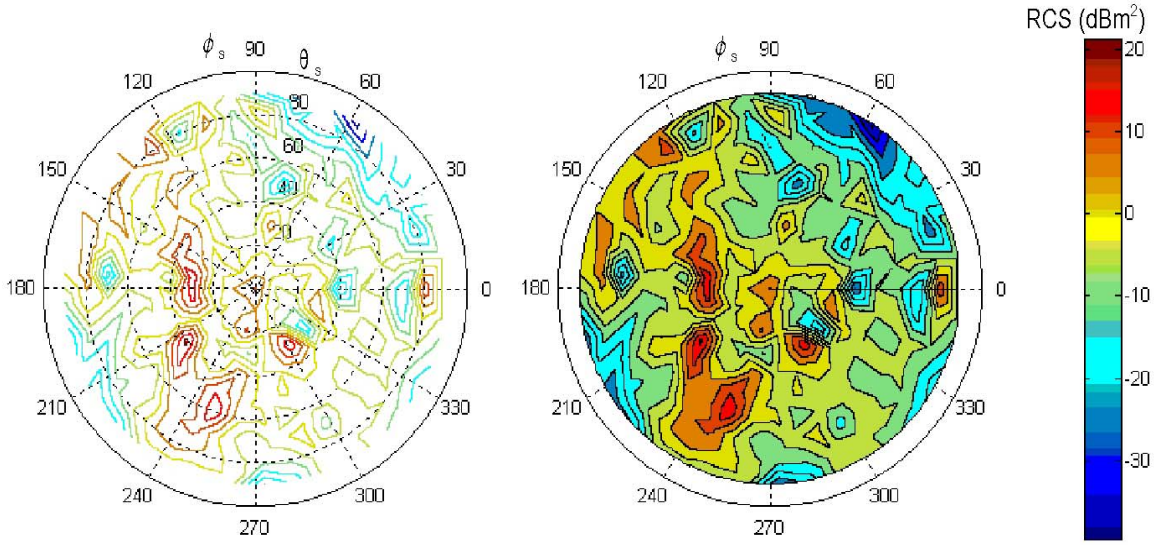

Figure 20. Scattering azimuth $\phi_s = 60°$

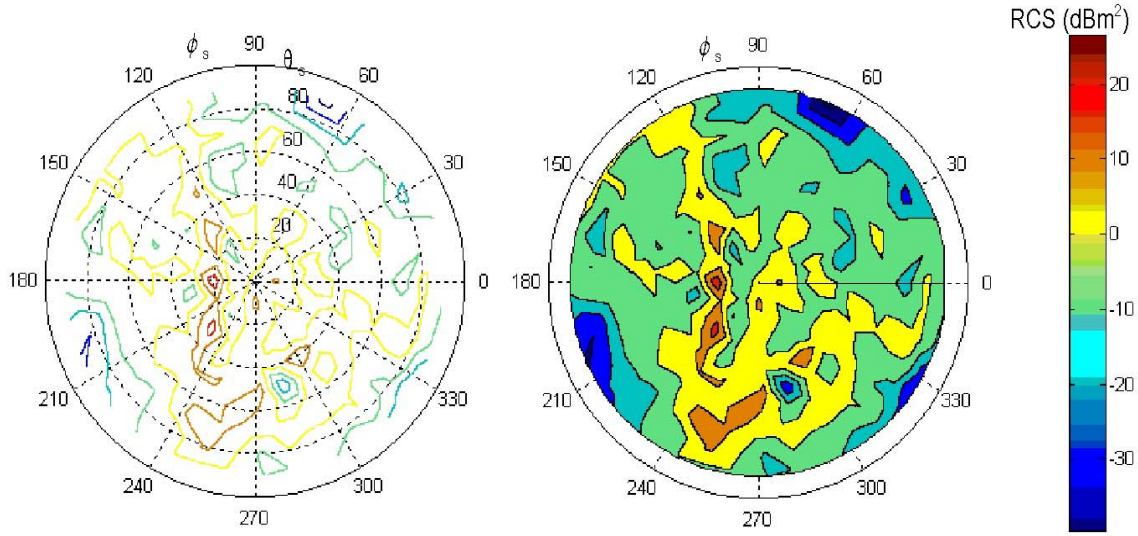

Figure 21. Scattering azimuth $\phi_s = 70°$

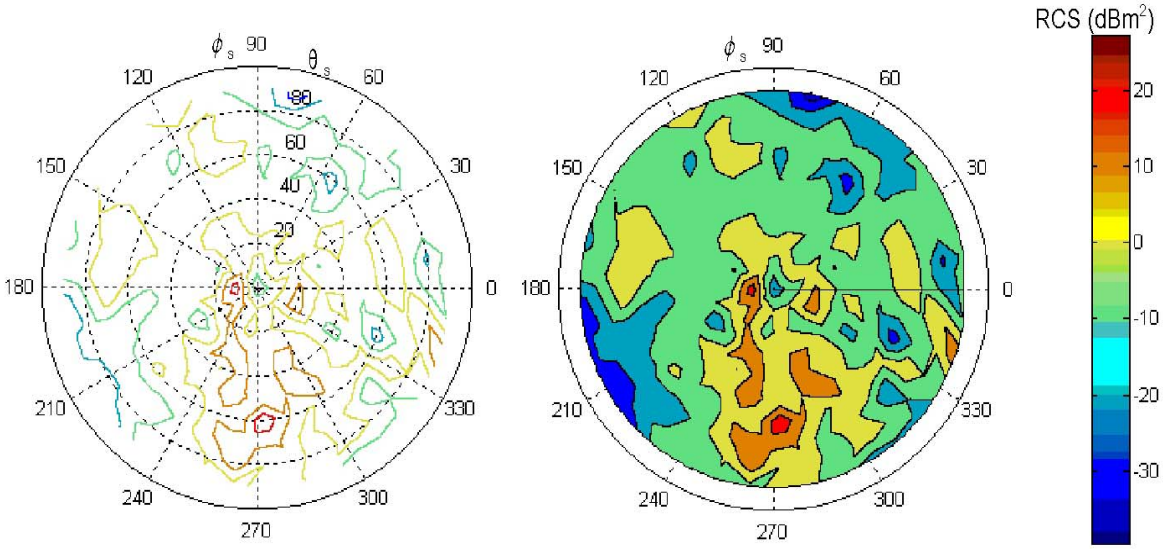

Figure 22. Scattering azimuth $\phi_s = 80°$

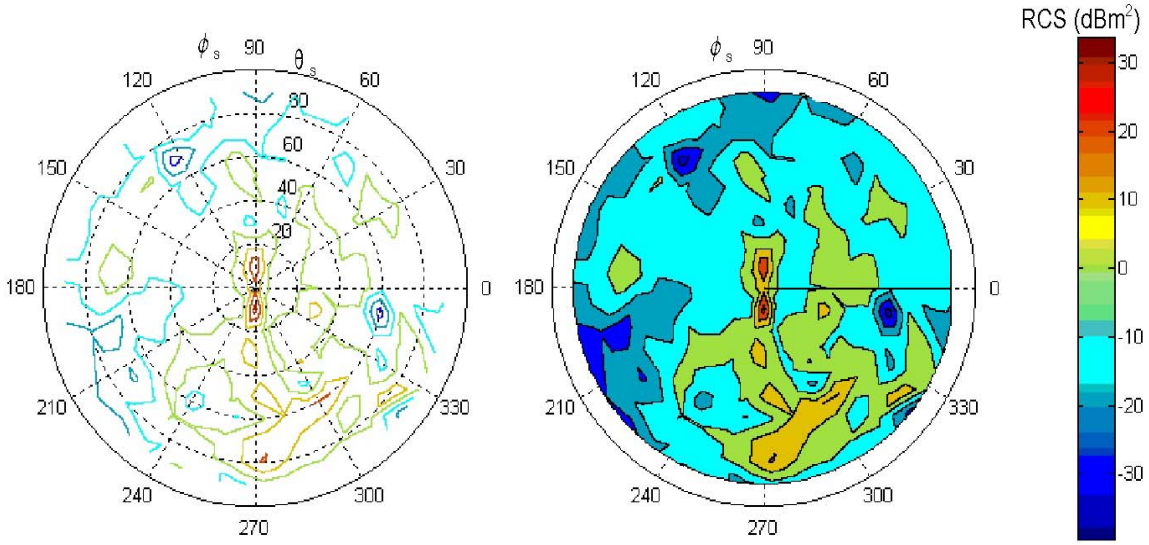

Figure 23. Scattering azimuth $\phi_s = 90°$

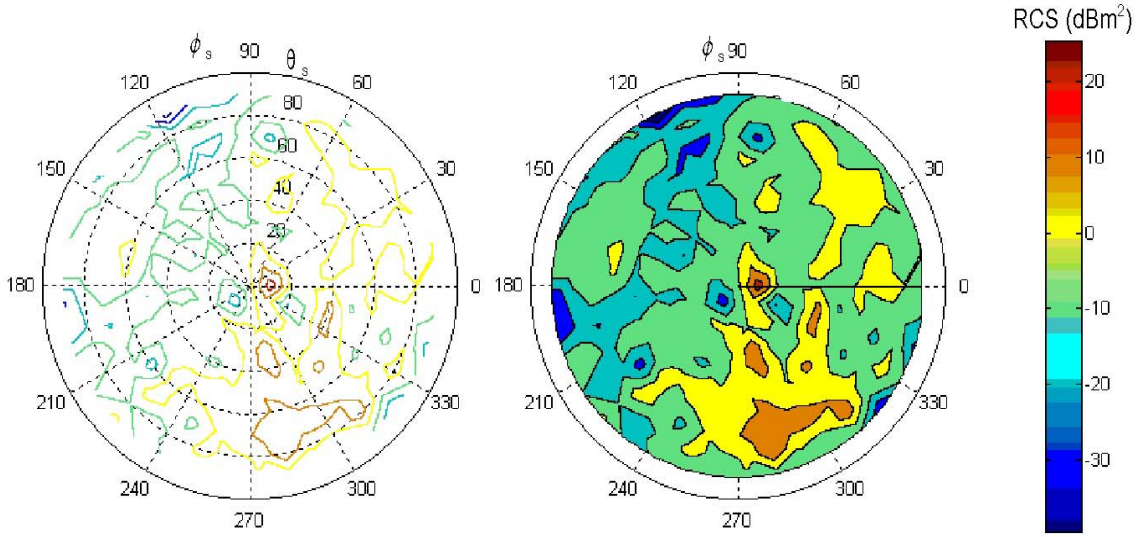

Figure 24. Scattering azimuth $\phi_s = 100°$

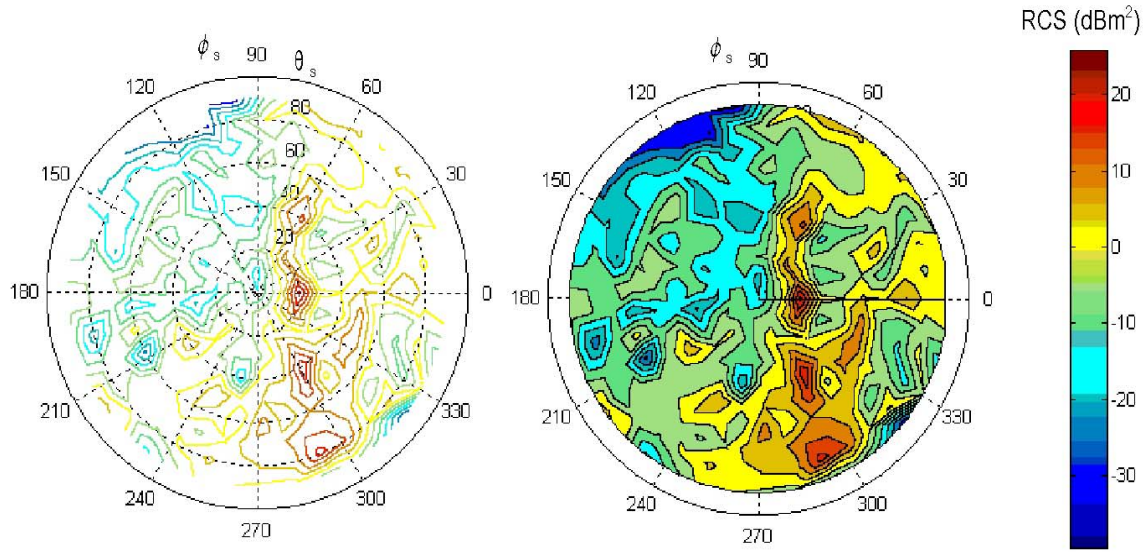

Figure 25. Scattering azimuth $\phi_s = 110°$

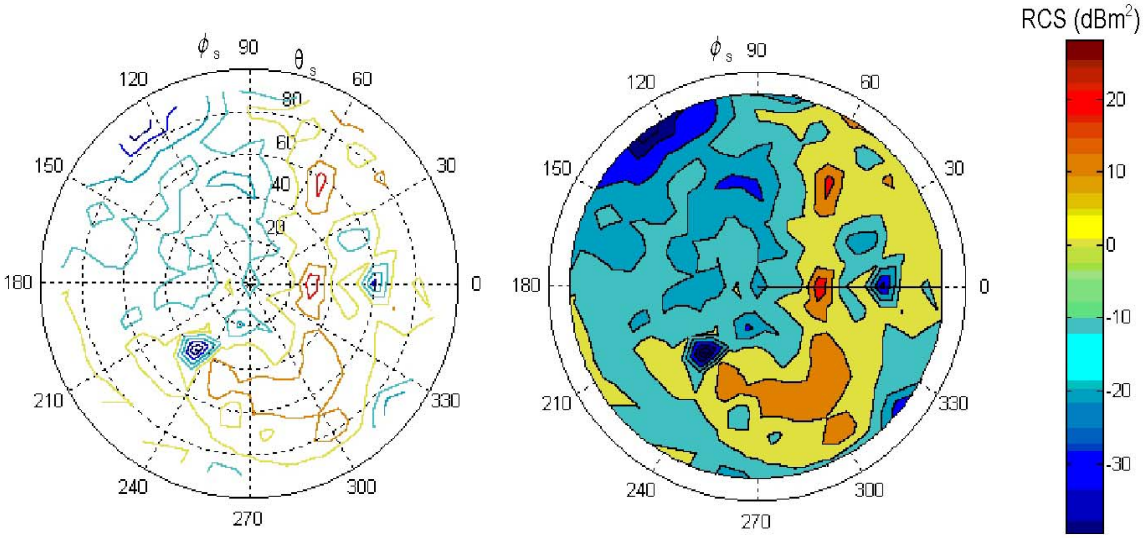

Figure 26. Scattering azimuth $\phi_s = 120°$

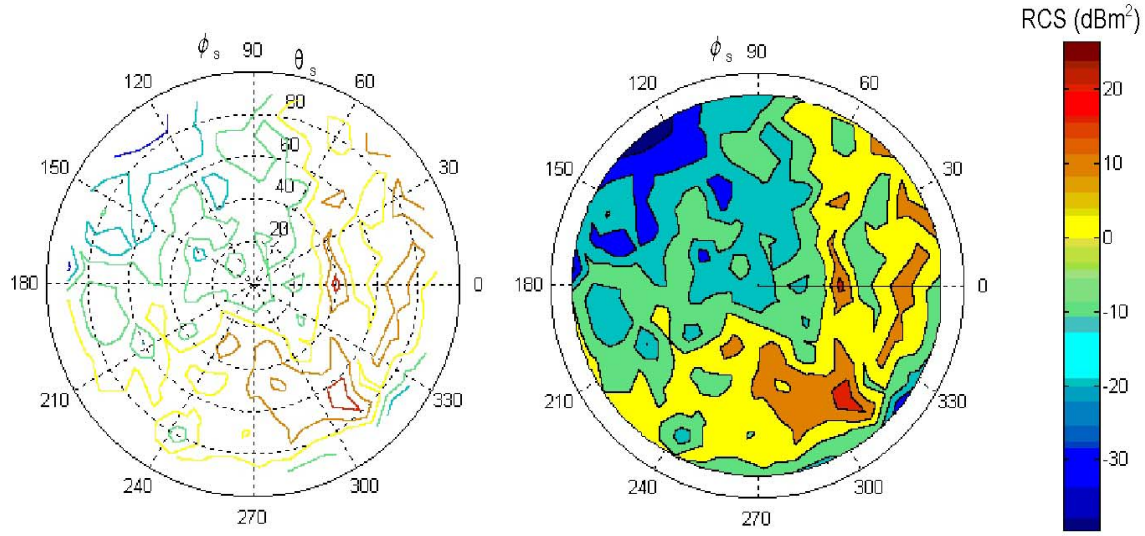

Figure 27. Scattering azimuth $\phi_s = 130°$

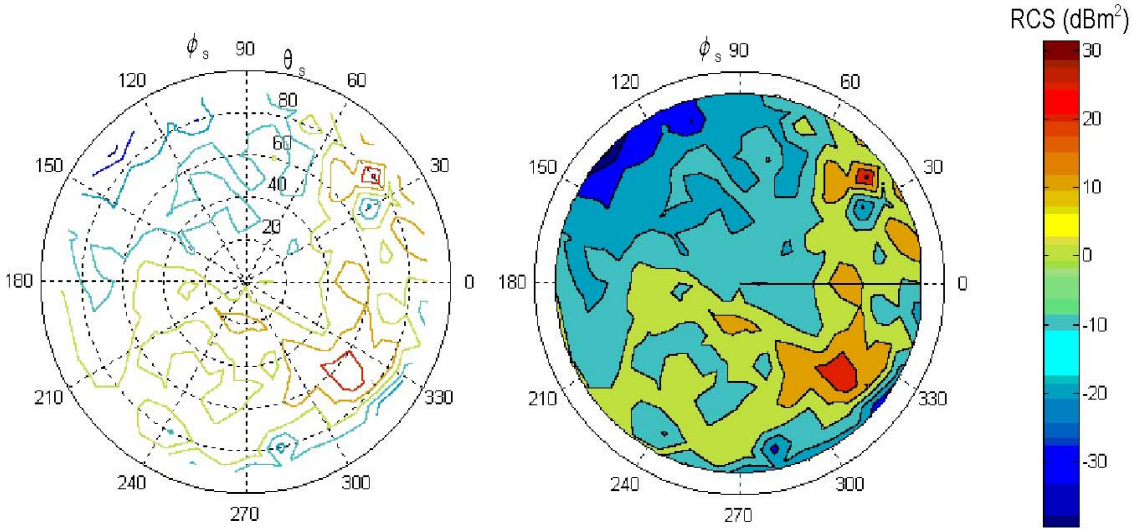

Figure 28. Scattering azimuth $\phi_s = 140°$

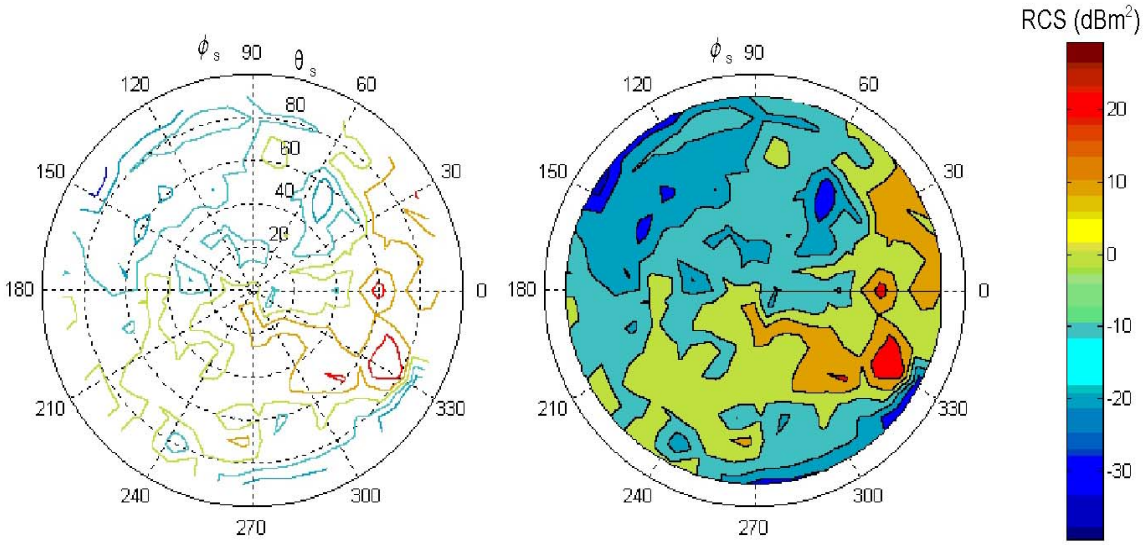

Figure 29. Scattering azimuth $\phi_s = 150°$

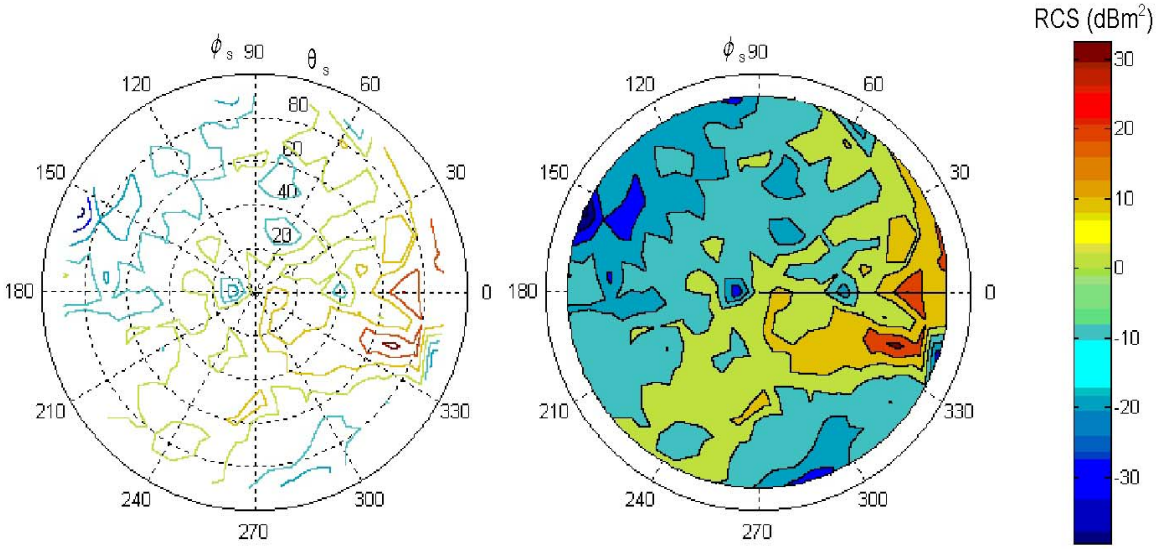

Figure 30. Scattering azimuth $\phi_s = 160°$

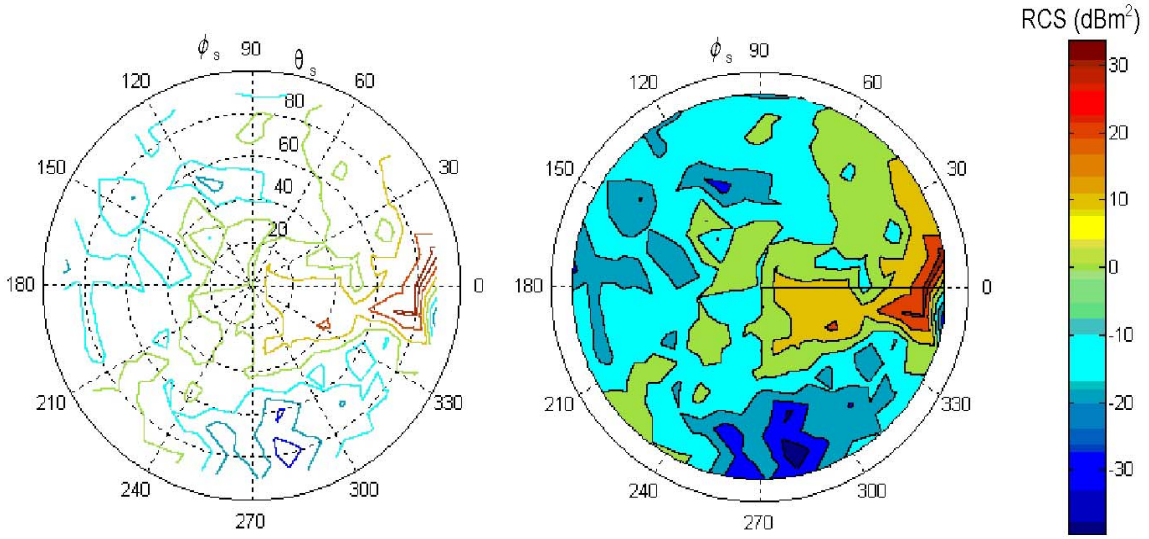

Figure 31. Scattering azimuth $\phi_s = 170°$

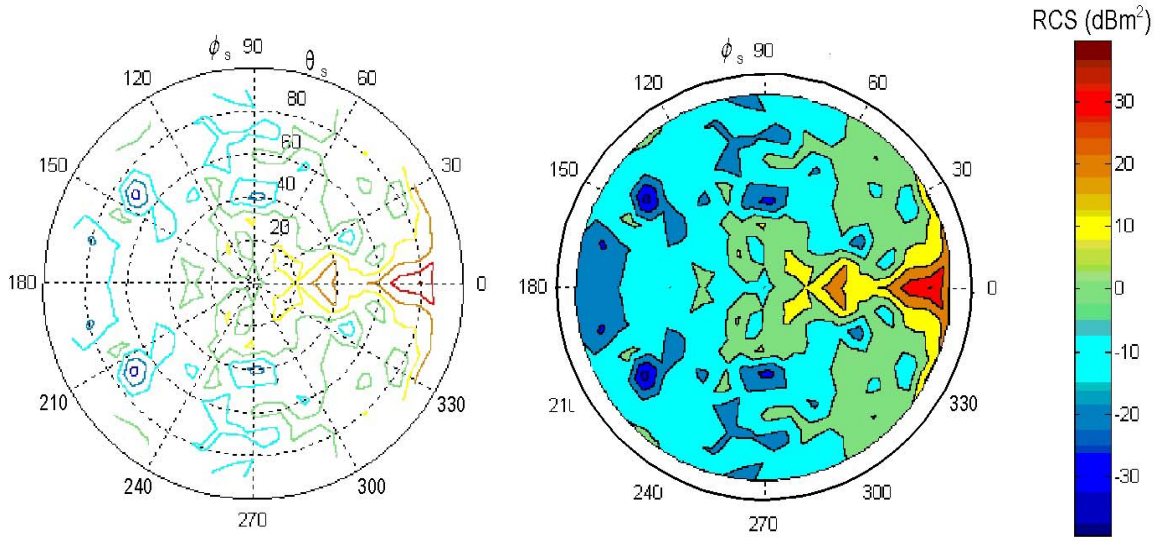

Figure 32. Scattering azimuth $\phi_s = 180°$

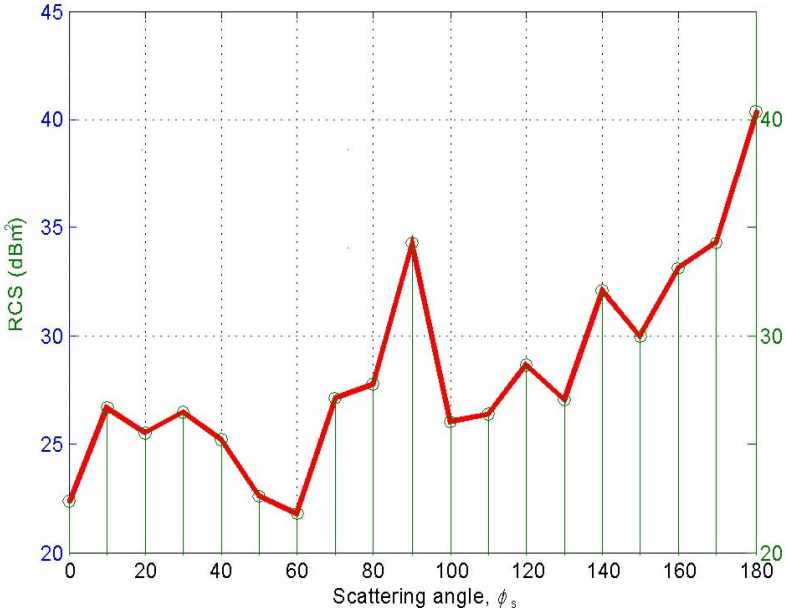

Figure 33. Summary of maximum RCSs for each scattering angle, ϕ_s.

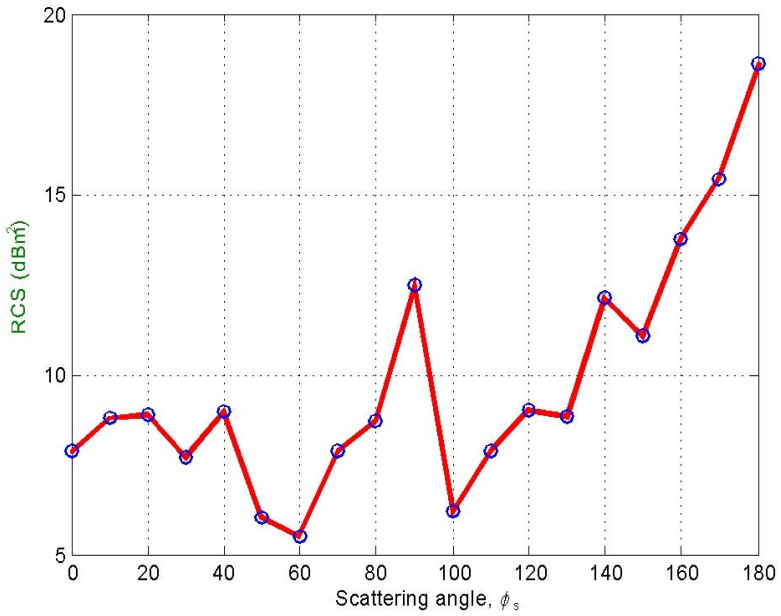

Figure 34. Summary of average RCSs for each scattering angle, ϕ_s.

ANNEX. Physical Optics (PO) Simulation

PO assumes that the field incident on the surface of the scattering body is the geometrical optics (GO) field at each point on its illuminated side. The scattering surface is discretized by subdividing it into smaller elements. The criterion for surface subdivision should be one that allowed, in the worst case, a phase difference of $\pi/4$, or equivalently a separation between surface elements or patches of at most $\lambda/8$.

Scattering is assumed in PO to take place as if there were an infinite tangent plane at each point, while over the shadowed regions of the scatterer the field at the surface is assumed to be zero [3].

For a perfectly conducting body, the assumed PO surface current is given by

$$\vec{\mathrm{J}}_{\mathrm{PO}} = \begin{cases} \hat{n} \times \vec{H}_{\mathrm{T}} & \text{in the illuminated region} \\ 0 & \text{in the shadowed region} \end{cases}$$

with $\hat{n}$ the unit normal vector to the scattering surface. From image theory, the tangential components of the current on a perfect electrical conductor are given by

$$\vec{\mathrm{J}}_{\mathrm{PO}} = 2(\hat{n} \times \vec{H}_i) \,.$$

The PO scattered field is given by the integral

$$\vec{H}_s \approx \iint_{\text{Lit surface}} \frac{\mathrm{j}k}{4\pi R} (\vec{\mathrm{J}} \times \vec{R}) e^{\mathrm{j}k\vec{R}} ds'$$

where $\vec{R}$ is the vector from each surface element to the receiver and R is the distance.

The scattered field from each surface element of area, Δs, can be computed using the vector potential $\vec{A}$,

$$\vec{A} = \frac{\mu}{4\pi} \vec{\mathrm{J}}_{\mathrm{PO}} \frac{e^{-\mathrm{j}kR}}{R} \Delta s \,.$$

Normally, an auxiliary vector, $\vec{N}$, is used where

$$\vec{N} = \vec{\mathrm{J}}_{\mathrm{PO}}\, e^{-\mathrm{j}kR}\Delta s\,.$$

The scattered field for each surface element can be computed from $\vec{A}$ using the expression,

$$\vec{E} = -\mathrm{j}\omega\left[\vec{A} + \frac{1}{k^2}\nabla\left(\nabla\cdot\vec{A}\right)\right],$$

where, for sufficiently large distances, the terms of order $1/R^2$, $1/R^3$, etc. can be neglected while the terms in $1/R$ are kept. These last components are contained in the first term of the above equation. Thus,

$$\vec{E}_\theta \approx -\mathrm{j}\omega\vec{A}_\theta \quad \text{and} \quad \vec{E}_\phi \approx -\mathrm{j}\omega\vec{A}_\phi\,.$$

In terms of $\vec{N}_\theta$ and $\vec{N}_\phi$,

$$\vec{A}_\theta = \frac{\mu}{4\pi R}\vec{N}_\theta \quad \text{and} \quad \vec{A}_\phi = \frac{\mu}{4\pi R}\vec{N}_\phi\,.$$

The scattered field is then given by

$$\vec{E}_\theta \approx -\frac{\mathrm{j}k}{4\pi R}\eta\vec{N}_\theta \quad \text{and} \quad \vec{E}_\phi \approx -\frac{\mathrm{j}k}{4\pi R}\eta\vec{N}_\phi$$

where η is the propagation media impedance, i.e., 120π.

Right hand circular polarization (RHCP) was used with polarization vector $(\hat{\theta} + \mathrm{j}\hat{\phi})/\sqrt{2}$. Assuming that the surface scattering element is located on the XY plane, we have that the incoming θ component gives rise to the following currents, auxiliary vectors and scattered fields:

$$\vec{\mathrm{J}}_{\mathrm{PO}} = 2\,\hat{z}\times\left(\cos\theta_i\cos\phi_i\hat{x} + \cos\theta_i\sin\phi_i\hat{y} - \sin\theta_i\hat{z}\right) = 2\hat{y}\cos\theta_i\cos\phi_i - 2\hat{x}\cos\theta_i\sin\phi_i = \mathrm{J}_y\hat{y} + \mathrm{J}_x\hat{x}\,,$$

$$\vec{N}_\phi = \left(\mathrm{J}_x\cos\theta\cos\phi + \mathrm{J}_y\sin\phi\cos\theta\right)e^{-\mathrm{j}kR}\Delta s\,,$$

$$\vec{N}_\phi = \left(-\mathrm{J}_x\sin\phi + \mathrm{J}_y\cos\phi\right)e^{-\mathrm{j}kR}\Delta s\,,$$

$$\vec{E}_{\theta\theta} = -\frac{\mathrm{j}k}{4\pi R}\eta\,\left(\mathrm{J}_x\cos\theta\cos\phi + \mathrm{J}_y\cos\theta\sin\phi\right)e^{-\mathrm{j}kR}\Delta s\,,$$

$$\vec{E}_{\theta\phi} = -\frac{\mathrm{j}k}{4\pi R}\eta\left(-\mathrm{J}_x\sin\phi + \mathrm{J}_y\cos\phi\right)e^{-\mathrm{j}kR}\Delta s\,.$$

$\vec{E}_{\theta\theta}$ means θ component due to incident θ field and $\vec{E}_{\theta\phi}$ means ϕ component due to incident θ field.

Using the same approach, the fields due to the ϕ component of the incident field can be calculated. Only the PO current is given, i.e.,

$$\vec{\mathrm{J}}_{\mathrm{PO}} = 2\hat{z}\times\left(-\sin\phi_i\hat{x} + \cos\phi_i\hat{y}\right) = -2\sin\phi_i\hat{y} - 2\cos\phi_i\hat{x} = \vec{\mathrm{J}}_y\hat{y} + \vec{\mathrm{J}}_x\hat{x}\,.$$

From this current the two components of scattered field $\vec{E}_{\phi\theta}$ and $\vec{E}_{\phi\phi}$ can be computed. The total fields originated by the θ and ϕ components of the incident field are given by

$$\vec{E}_\theta^{\,T} = \frac{\vec{E}_{\theta\theta} + \mathrm{j}\vec{E}_{\phi\theta}}{\sqrt{2}} \quad \text{and} \quad \vec{E}_\phi^{\,T} = \frac{\vec{E}_{\theta\phi} + \mathrm{j}\vec{E}_{\phi\phi}}{\sqrt{2}}$$

and the total scattered field is

$$\vec{E}^{\,T} = \vec{E}_\theta^{\,T} + \vec{E}_\phi^{\,T} = \frac{\vec{E}_{\theta\theta} + \vec{E}_{\theta\phi} + \mathrm{j}(\vec{E}_{\phi\theta} + \vec{E}_{\phi\phi})}{\sqrt{2}}\,,$$

which, in general, corresponds to an elliptical polarization.

In order to apply the above integral, the lit part of the scattering is split into small triangular patches to approximate the curved surface of the aircraft. Figure A.1 illustrates this approach. The

contributions from each patch is a Dirac delta with a given amplitude, phase, delay and polarization in the channel impulse response,

$$h(\tau) = E_0(\tau - \tau_0) + \sum E_i(\tau - \tau_i),$$

where the component with subscript 0 is the direct ray and those with subscript *i* are the scattered contributions. The various phenomena at the receiver, e.g., coherent sum of closely delayed field components were considered to take into account the delay resolution capabilities of the channel sounder used in the measurements.

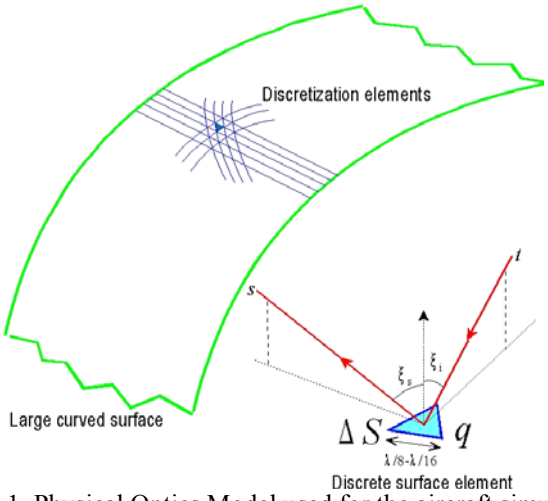

Figure A.1. Physical Optics Model used for the aircraft simulations.

3 THE TAXIING SCENARIO. STATISTICAL MODELING

Figure 35 illustrates a simple, one-runway airport configuration. Based on this simple layout, this channel model assumes a number of aircraft in sequence toward the runway. As shown in Figure 36, the victim receiver is aircraft (1) which is somewhere queuing up along the taxiway. Two other aircraft, one in front (2) and one in back (3) are the foreground taxiway (FG-TW) model elements. Four additional aircraft (4), (5), (6) and (7) make up the background (BG-TW) model elements. Further, an aircraft (8) is assumed to be taking off on the runway (FG-RW) abreast of the victim aircraft.

In addition to the direct signal, multipath contributions come from the victim aircraft (1) itself, and from the other aircraft: (2)-(8).

The various taxiing aircraft on this generic scenario are nominally separated by 90 m with a variation of ±10 m. The minimum distance between the victim and the aircraft on the runway taking off is 150 m.

One further model element is the ground contribution (9). It is assumed that the surface of the airport is smooth and thus, its diffuse multipath contribution is negligible compared to the others. Specular reflections will only be significant for circular polarization when below the Brewster angle which is for an elevation angle of about 5º.

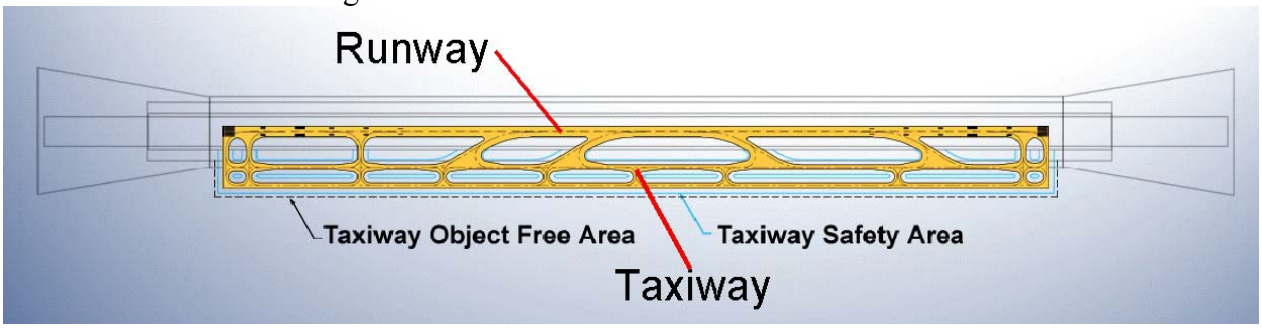

Figure 35. Airport layout: taxiway and runway configuration.

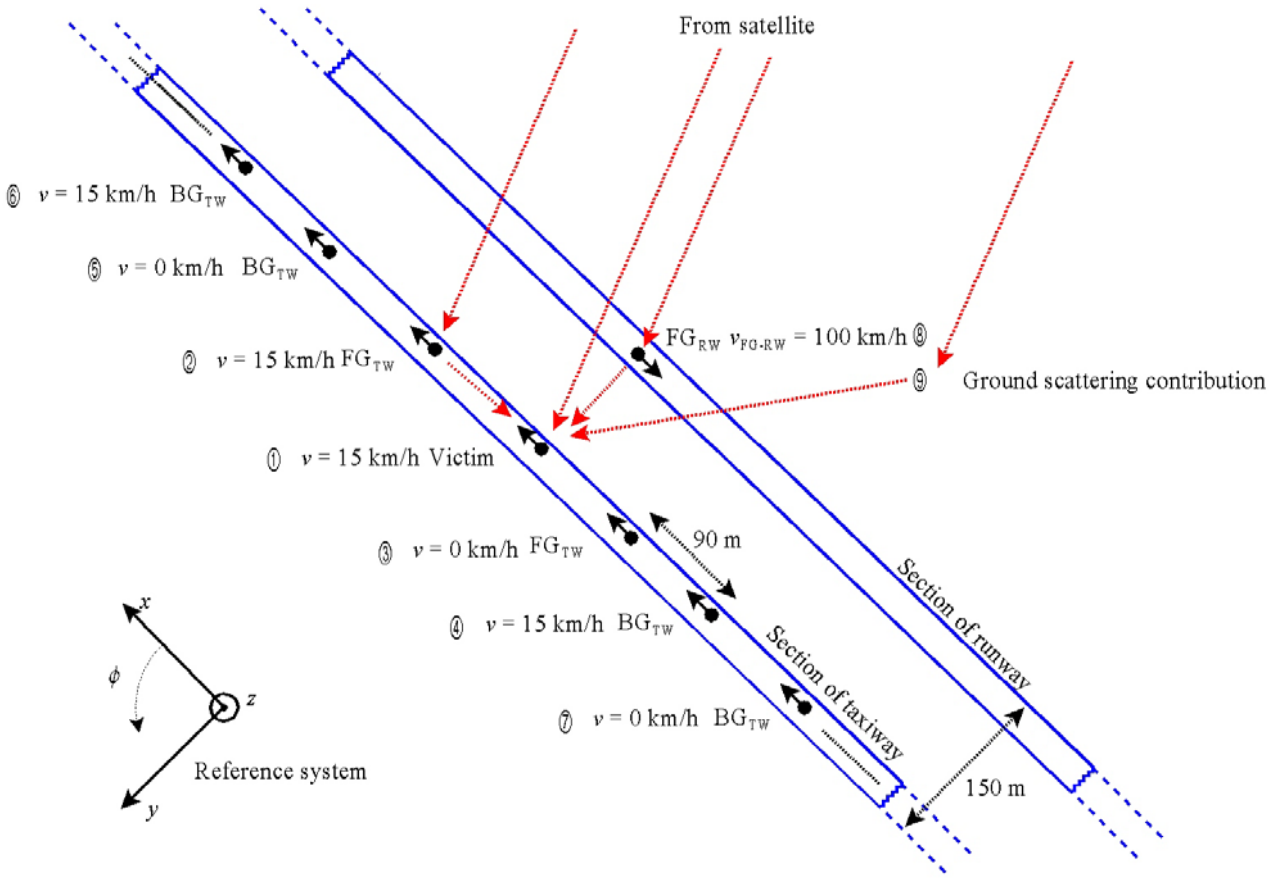

Figure 36. Schematic diagram of taxiing channel model.

Regarding mobility, some of the taxiing aircraft are assumed to be moving at a speed of 15 km/h while others have momentarily stopped. The aircraft taking off is at a speed of 100 km/h when closest to the victim. Mobility induces both Doppler shift and spread. In turn, Doppler spread gives rise to fading.

In the case of a static transmitter and scatterer, and a mobile receiver, the Doppler shift introduced by the moving receiver is given by

$$f_D = \frac{v_1}{\lambda}\cos(\alpha_1)$$

where v_1 is the speed of the aircraft and α_1 is the incidence angle of the radio path with respect to the mobile trajectory.

Doppler modeling in the case in hand is more complex given that the satellite is not geostationary, and the aircraft taking off is a moving scatterer. In the model, in a first step the satellite Doppler shift is assumed to be compensated for at the receiver. In a second step, the Doppler introduced by the victim's movement is also removed.

In case of a moving scatterer and a moving receiver while the transmitter is stationary is given by

$$f_D = \frac{v_0 - v_1}{\lambda}\cos(\alpha_{10}) + \frac{v_1}{\lambda}\cos(\alpha_{t1})$$

where v_1 and v_2 are the speed of the victim aircraft and a moving aircraft, and α_{10} and α_{t1} are the corresponding incidence angles of the radio paths with respect to their trajectories (Figure 37).

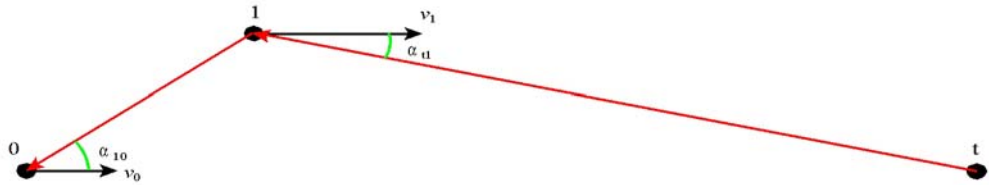

Figure 37. Doppler shift when the mobile and the scatterer are moving.

Additionally, due to the vibrations in the aircraft's external parts causing small relative changes between its various parts: wings, body, etc. a small amount of Doppler spread arises. It was assumed that the slowly moving airplanes suffer a spread of the order on ±1 Hz while the faster, taking off plane suffers a spread of ±20 Hz. The momentarily stationary airplanes do not cause Doppler spread.

Assuming a carrier frequency of 1500 MHz, the results of the two steps mentioned above regarding Doppler shifts are summarized in Figure 38.

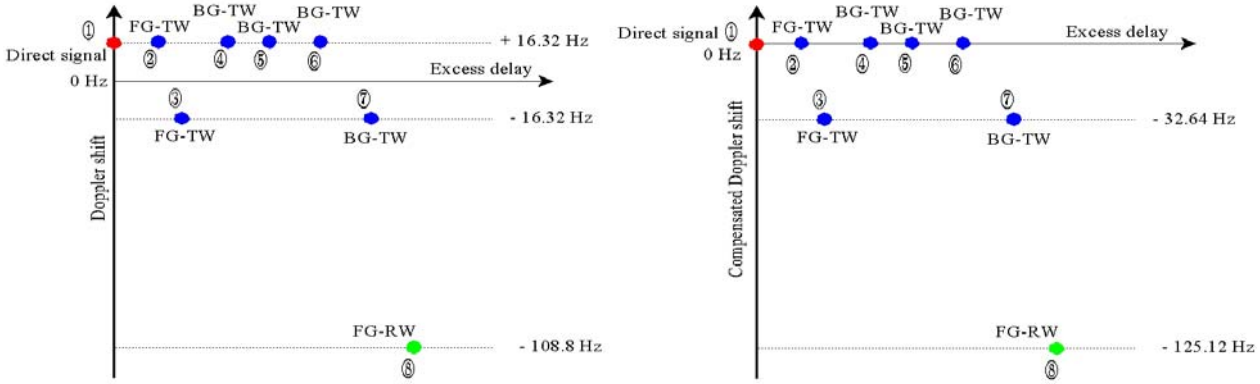

Figure 38. Doppler shifts before and after removing direct signal's shift. Satellite shift removed.

Regarding excess delays, the simplification is made that the illuminating signals from the satellite reaching the victim and the other aircraft are parallel. This simplifies the calculation of excess delays as illustrated in Figure 39. One further simplification consists of assuming that all scattered contributions from a given airplane are uniformly distributed in a range of delays defined by the size of the aircraft. In this case, the distribution is over 0.2 μs. Figure 40 shows one such distribution of contributions where the assumption is proven to be fairly accurate.

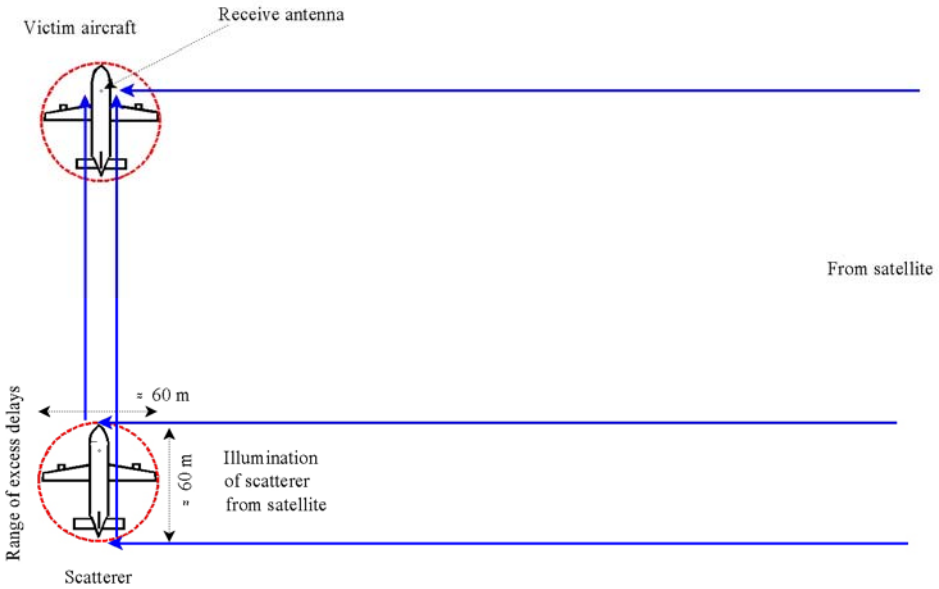

Figure 39. Calculation of excess delays assuming illuminating rays are parallel.

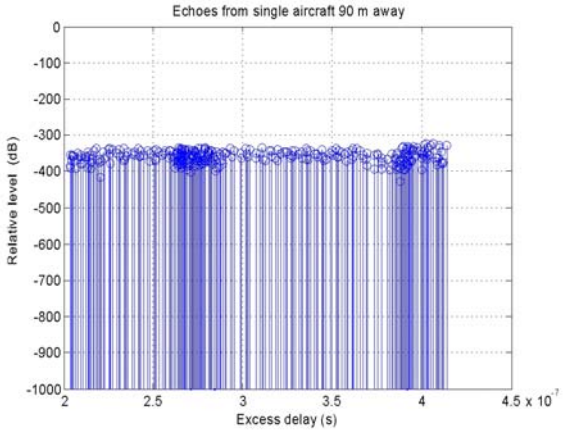

Figure 40. Distribution of echoes from the test aircraft 90 m away.

Now all elements are ready to be assembled into a full model. Table 1 summarizes all contributions with their corresponding excess delays, Doppler shift and spread, etc. Two worst case RCS values 30 and 40 dBm^2 have been used, the latter being an extremely high value, not realistic that all scatterers have such high value at the same time.

For calculating the received power from each aircraft the bi-static radar equation is used, i.e.,

$$\frac{p_r(\text{aircraft scattered})}{p_t} = g_t \cdot \frac{1}{4\pi d_1^2} \cdot \sigma \cdot \frac{1}{4\pi d_2^2} \cdot \frac{\lambda^2}{4\pi} g_r$$

where d_1 and d_2 are the distances from the satellite to the scatterer (aircraft) and from the scatterer to the victim. For the direct signal, the free space loss link budget is used assuming that d_0, the distance from the satellite to the victim is approximately the same as the d_1 values for the different aircraft. In this case,

$$\frac{p_r(\text{direct signal})}{p_t} = g_t \cdot \frac{1}{4\pi d_1^2} \cdot \frac{\lambda^2}{4\pi} g_r \,.$$

Then, the relative power of the multipath from a given aircraft with respect to the direct signal is

$$\frac{p_r(\text{aircraft scattered})}{p_r(\text{direct signal})} = \frac{\sigma}{4\pi d_2^2} \,.$$

This expression is valid when the direct signal and the scattered signal arrive with the same elevation angle, i.e., θ_s=90º. This will not normally be the case and the carrier-to-multipath ratio must be corrected (increased) according to the antenna mask values in Figure 1. Figure 41 summarizes all model contributions listed in Table 1, classified in terms of their excess delays and relative powers.

Table 1. Summary of model contributions.

Scatterer	Excess delay tap center (μs)	Excess delay range(μs)	Relative power RCS=30dB	Relative power RCS=40dB	Doppler Shift (Hz)	Doppler Spread (Hz)	Corrected Shift (Hz)
1	0.0	0-0.1	-17	-17	16.32	1	0
2	0.3	0.2-0.4	-20	-10	16.32	1	0
3	0.33	0.23-0.43	-21	-11	-16.32	0	-32.64
8	0.5	0.4-0.6	-24.5	-14.5	-108.8	20	-125.12
5	0.566	0.466-0.666	-25.6	-15.6	16.32	0	0
4	0.6	0.5-0.7	-26	-16	16.32	1	0
6	0.9	0.8-1.0	-29.6	-19.6	16.32	1	0
7	0.9333	0.833-1.033	-30	-20	-16.32	0	-32.64

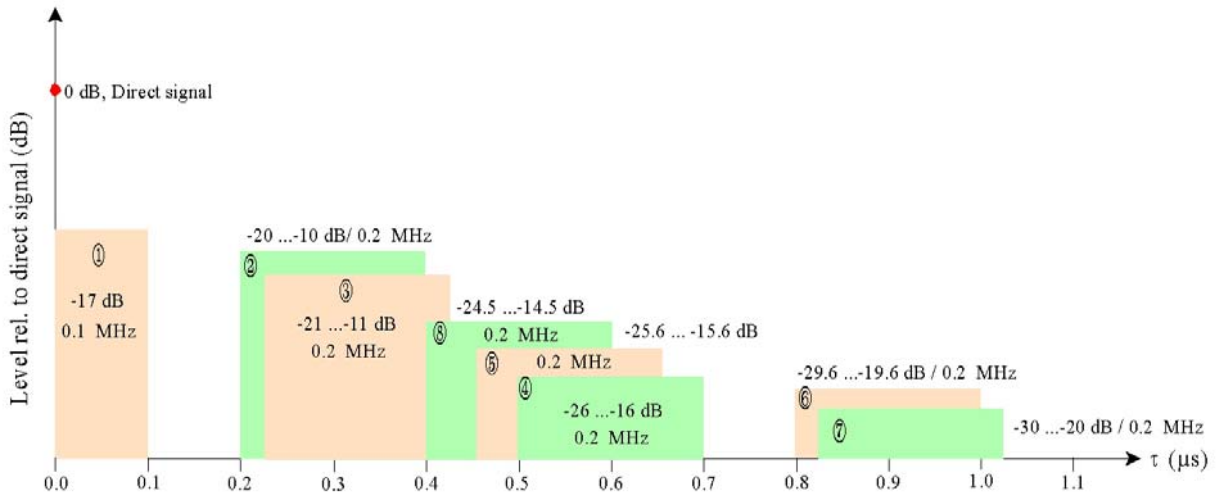

Figure 41. Channel model contributions according to their excess delays and relative powers.

4. TAPPED DELAY-LINE MODEL

In this section a wide-band channel model in the form of tapped delay-line, TDL, is developed from the model elements evaluated in the above section. A tap-spacing of 0.1 μs has been assumed, any other value can be taken and a similar TDL coefficient extraction procedure can be performed. Figure 42 illustrate the convolution of a sinc function of parameter $T = 0.1$ μs with the ideal impulse response calculated in the preceding section. The results of this processing are presented in Table 2. This table also provides the guidelines for implementing this channel model, i.e., for generating time-series.

In order to generate TDL time-series the generators in Figures 43 and 44 can be used. Figure 43 corresponds to a narrow-band channel while Figure 44 shows the wide-band channel of Figure 42 and Table 2 with a spacing between taps of 0.1 μs. Finally, Figures 45-55 present examples of time-series for all taps in the model.

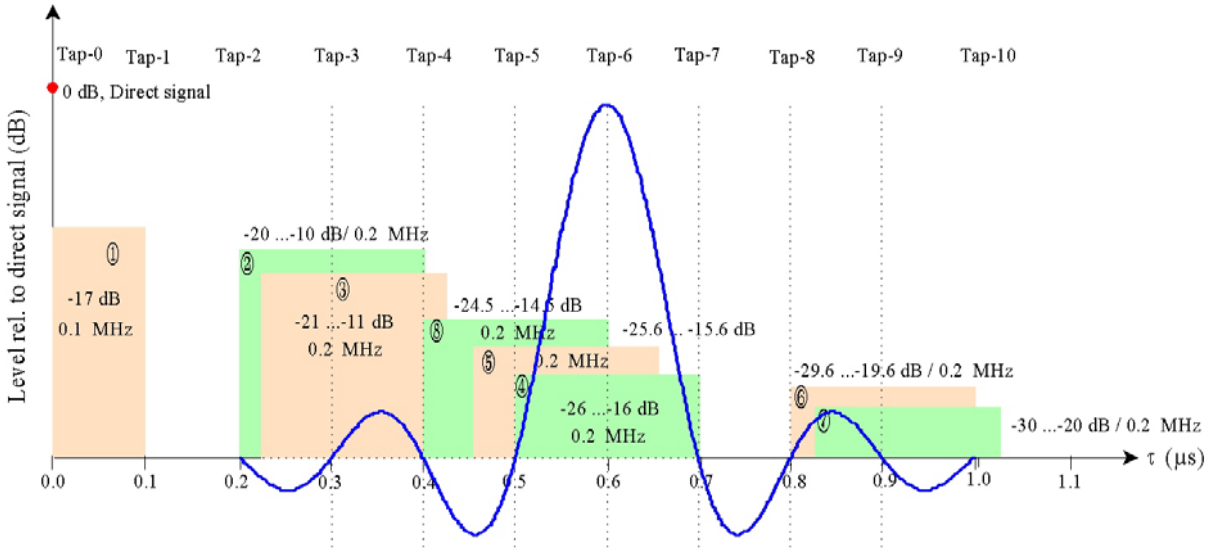

Figure 42. Channel model contributions according to their excess delays and relative powers classified in TDL taps.

Table 2. TDL model parameter for a spacing of 0.1 μs.

Tap #	Excess delay (μs)	Delay range (μs)	Contributions	Relative power (dB)	Total relative tap power (dB)	Doppler spread (Hz)	Doppler shift (Hz)

Tap-0	0.0	0-0.05	(1)	-20	-20	1	0
Tap-1	0.1	0.05-0.15	(1)	-20	-20	1	0
Tap-2	0.2	0.15-0.25	(2)(3)	-26/-31	-24.80	1/0	0/-32.64
Tap-3	0.3	0.25-0.35	(2)(3)	-23/-24	-20.47	1/0	0/-32.64
Tap-4	0.4	0.35-0.45	(2)(3)(8)	-26/-24.97/-30.52	-21.78	1/0/20	0/-32.64/-125.12
Tap-5	0.5	0.45-0.55	(8)(4)(5)	-27.5/-29.06/-32.02	-24.38	20/0/1	-125.1/0/0
Tap-6	0.6	0.55-0.65	(8)(4)(5)	-30.52/-28.61/-29.01	-24.53	20/0/1	-125.1/0/0
Tap-7	0.7	0.65-0.75	(5)(4)	-38.61/-32.02	-31.15	0/1	0/0
Tap-8	0.8	0.75-0.85	(6)(7)	-35.62/-40	-34.26	1/0	0/-32.64
Tap-9	0.9	0.85-0.95	(6)(7)	-32.61/-33.01	-29.79	1/0	0/-32.64
Tap-10	1	0.95-1.05	(6)(7)	-35.62/-33.97	-31.70	1/0	0/-32.64

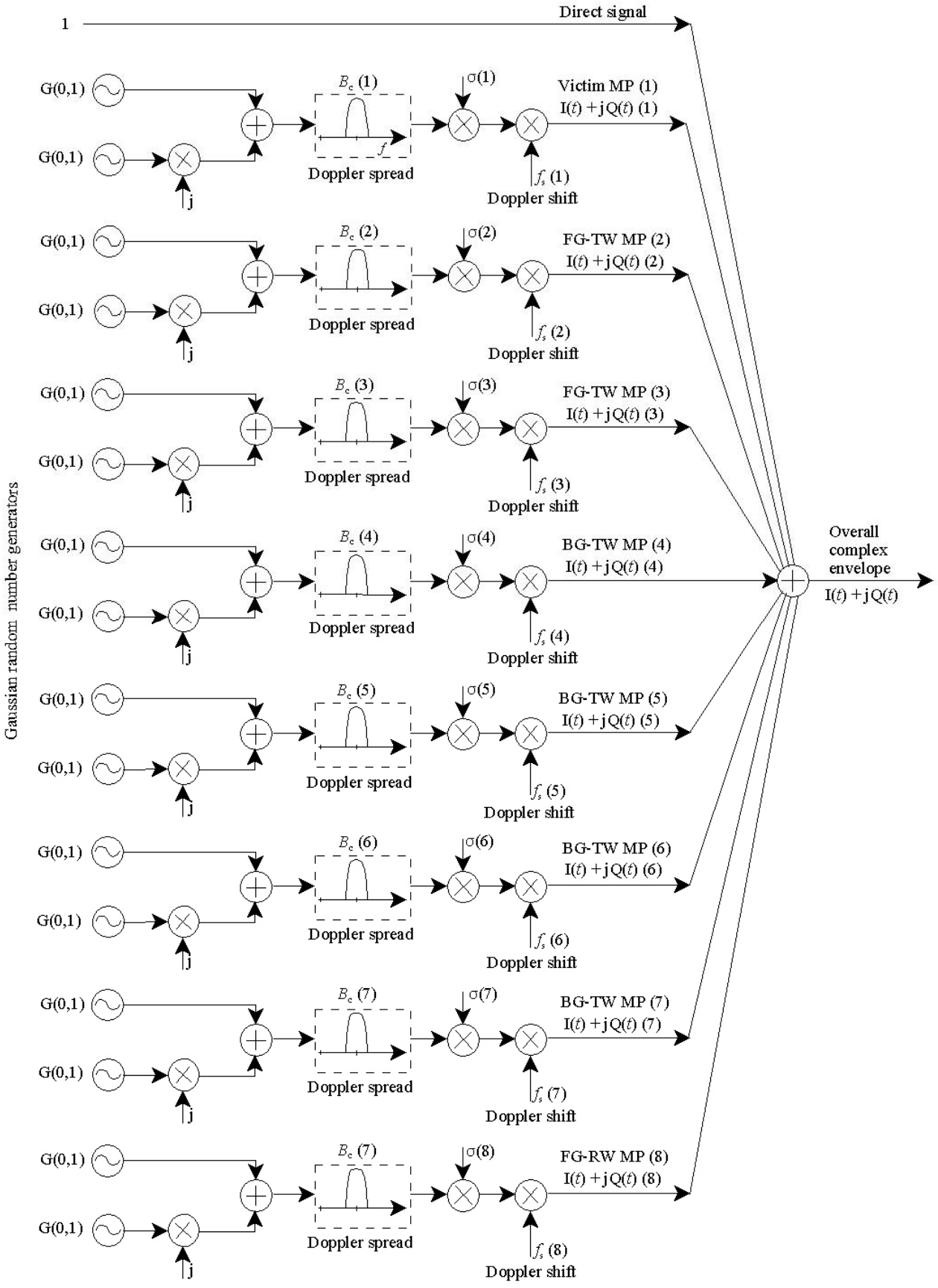

Figure 43. Circuital form of channel for generating simulation time series. Narrow-band model.

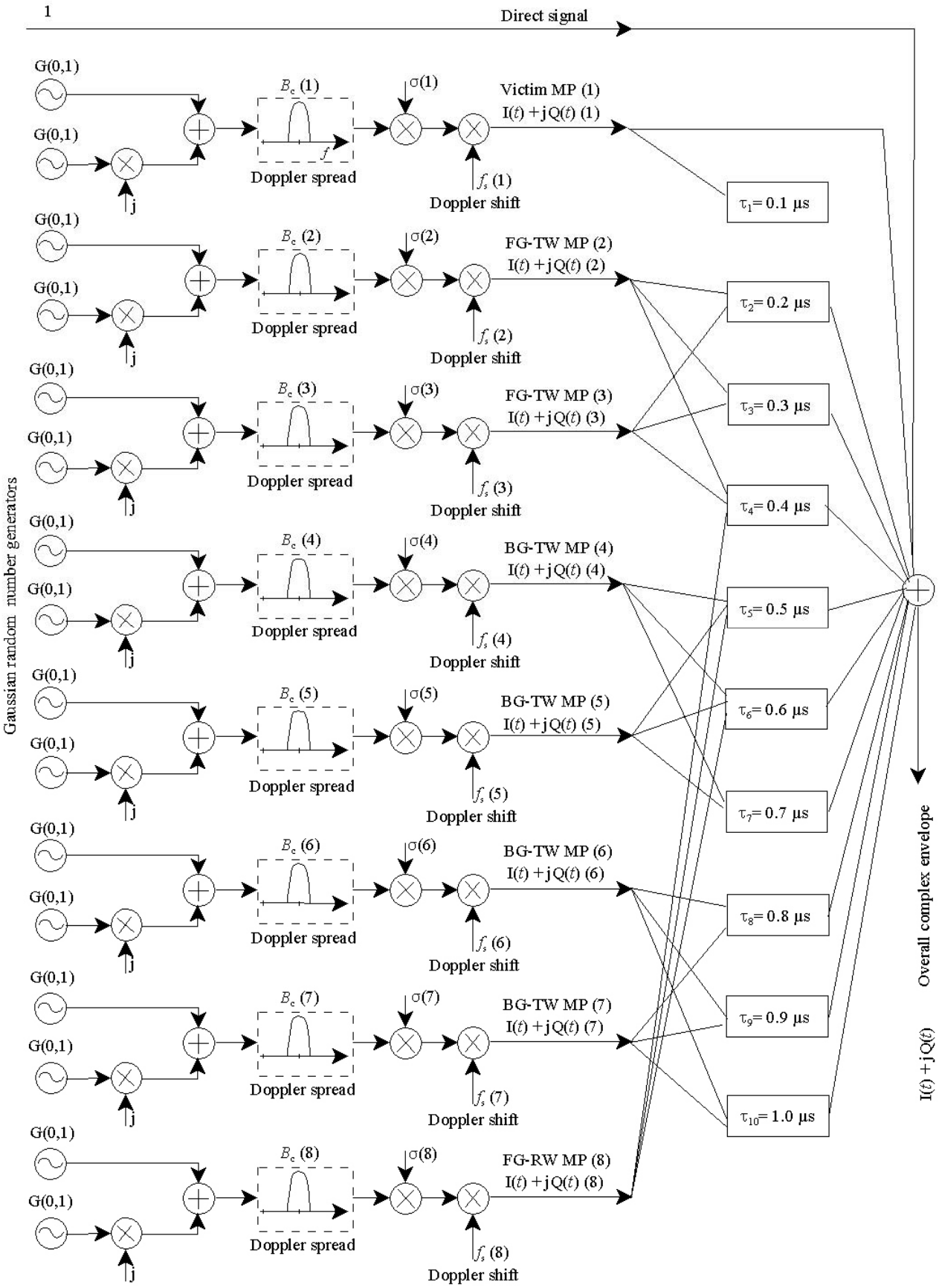

Figure 44. Circuital form of channel for generating simulation time series. Wide-band model.

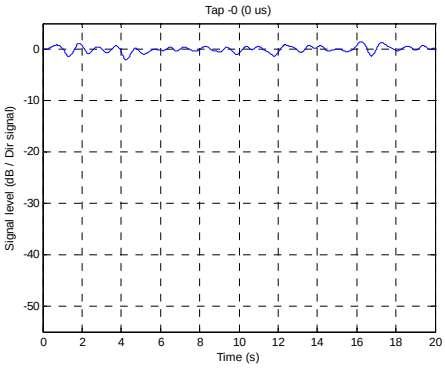

Figure 45. Time-series for Tap-0.

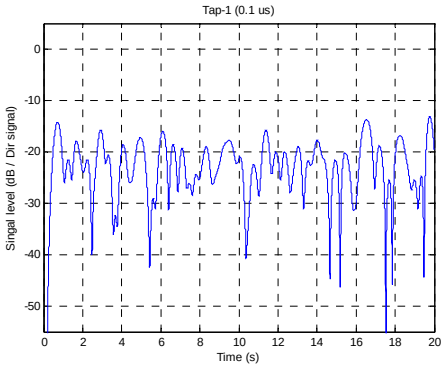

Figure 46. Time-series for Tap-1.

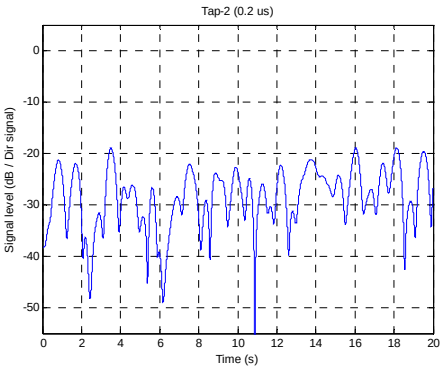

Figure 47. Time-series for Tap-2.

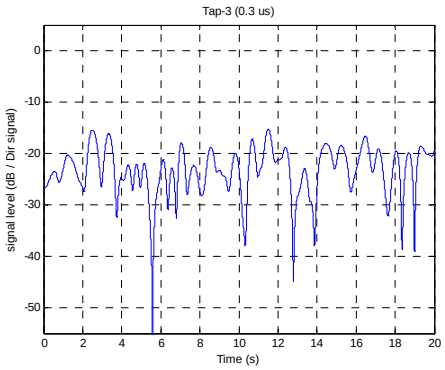

Figure 48. Time-series for Tap-3.

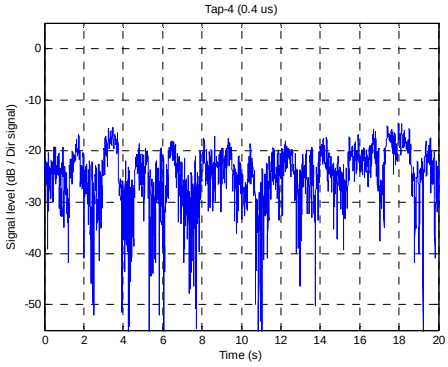

Figure 49. Time-series for Tap-4.

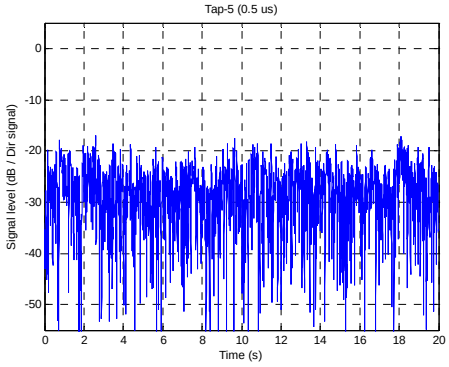

Figure 50. Time-series for Tap-5.

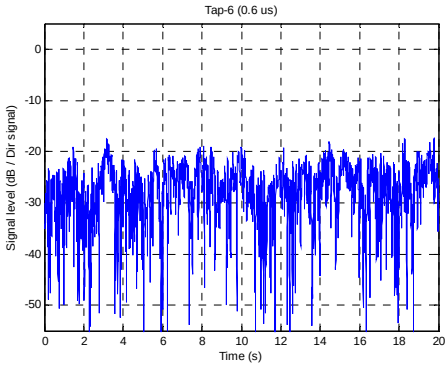

Figure 51. Time-series for Tap-6.

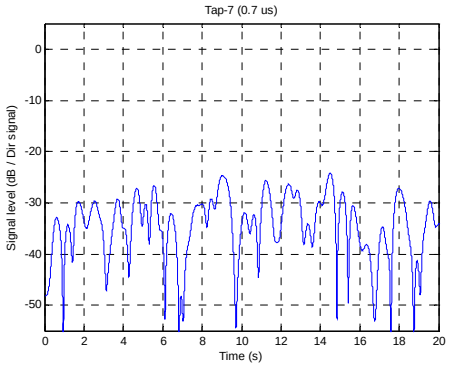

Figure 52. Time-series for Tap-7.

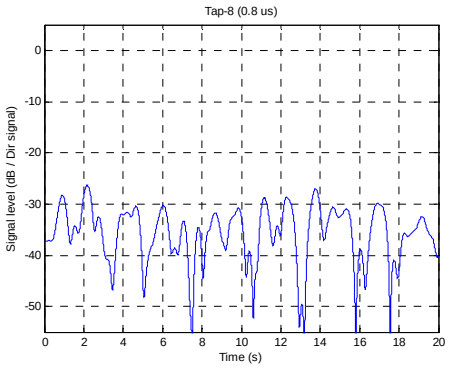

Figure 53. Time-series for Tap-8.

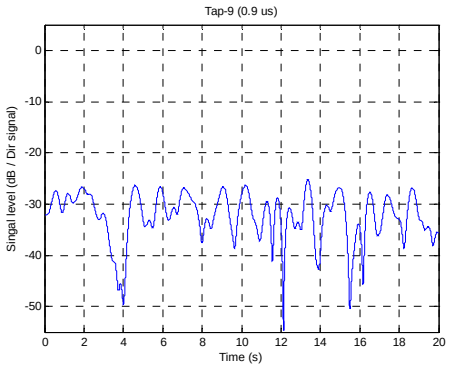

Figure 54. Time-series for Tap-9.

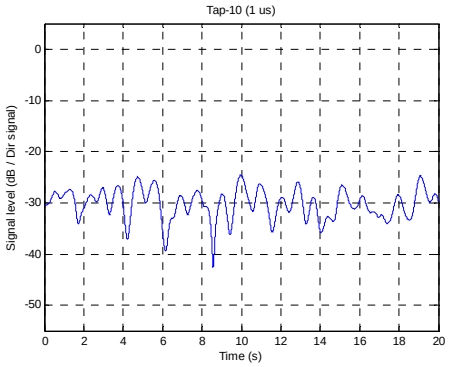

Figure 55. Time-series for Tap-10.

5 SUMMARY, CONCLUSIONS AND FURTHER WORK

In this paper a simplified taxiing channel model has been developed. This model is directly applicable in the production of synthetic time-series for simulation in the form of tapped delay-lines. This model can be made more complex by considering other contributions from different possible scatterers (vehicles, the terminal building, etc.) present in an airport. However, this is te moment of verifying whether the model assumptions and quantification of effects are valid through measurements.

6 REFERENCES

[1] Surface movement guidance and control system. Advisory circular AC No. 120-57A, 12/19/96. FAA.
[2] A.Jongejans et. al., Prosat Phase I Report. ESA STR-216, May 1986
[3] A.Steingass, A.Lehner, F.P.Fontan, E.Kubista, M.J.Martin, and B.Arbesser-Rastburg. The High Resolution Aeronautical Multipath Navigation Channel. ION NTM 2004 Conference, January 26-28, 2004, in San Diego, California USA.
[4] W.L.Stutzman and G.A.Thiele. Antenna Theory and design. John Wiley and sons., 1981.
[5] C.A.Balanis. Advanced Engineering Electromagnetics. John Wiley and sons., 1989.